

**Gravitomagnetic Effects in Compact Binary Systems:  
A Study of Spin-Enhanced Orbits around Kerr Black Holes**

by

Akash Pravin Kansagra

Submitted to the Department of Physics  
in partial fulfillment of the requirements for the degree of

Bachelor of Science

at the

MASSACHUSETTS INSTITUTE OF TECHNOLOGY

June 2004

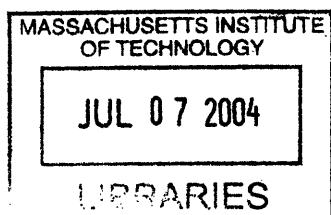
© Akash Pravin Kansagra, MMIV. All rights reserved.

The author hereby grants to MIT permission to reproduce and distribute publicly  
paper and electronic copies of this thesis document in whole or in part.

Signature of Author .....  
Department of Physics  
May 7, 2004

Certified by .....  
Professor Scott A. Hughes  
Assistant Professor, Department of Physics

Accepted by .....  
Professor David E. Pritchard  
Senior Thesis Coordinator, Department of Physics



**ARCHIVES**



**Gravitomagnetic Effects in Compact Binary Systems:  
A Study of Spin-Enhanced Orbits around Kerr Black Holes**

by

Akash Pravin Kansagra

Submitted to the Department of Physics  
on May 7, 2004, in partial fulfillment of the  
requirements for the degree of  
Bachelor of Science

**Abstract**

An important subject in current gravity research concerns the evolution of compact binary systems in which both members spin, particularly in the extreme mass ratio limit. Previous research has suggested that the effect of spin in such systems may be particularly significant—possibly even chaotic—near the homoclinic set of orbits, which lie close to the separatrix dividing stable and unstable orbits.

In this thesis we present a study of the spin-induced evolution of inclined, eccentric Kerr black hole orbits. The evolution of the orbital energy, angular momentum, and Carter constant for such orbits is driven by the local spin force on the orbiting body, which is inferred from the Papapetrou equations. We find that the variation of the constants which characterize the orbit (e.g., energy, angular momentum, and Carter constant) is complicated and occurs on orbital timescales, but is contained within well-defined bounds that expand smoothly as the spin on the orbiting body is increased. As a consequence, the total volume explored in the orbital phase space of a given orbit is finite. We also find that the phase space volume grows rapidly as one approaches the homoclinic set of orbits, but ceases to increase once the particle comes within a certain threshold distance of the separatrix.

Thesis Supervisor: Professor Scott A. Hughes  
Title: Assistant Professor, Department of Physics



## Acknowledgments

Achieving a degree in physics from MIT represents the accomplishment of a major life goal. In its attainment I have invested my entire being, but I would certainly have fallen short of the finish line were it not for the help and support of others. My family especially can take credit for my success. Their unwavering faith in me, from a very early age, was truly empowering. By placing such tremendous confidence in me and my often adventurous decisions, they gave me the greatest gift of all: the ability to set and achieve my own goals.

I also owe a debt of gratitude to my friends from Southern California. As a student at Troy High School, I had the privilege to study alongside and under some of the kindest and most intelligent individuals I have ever met. I learned a lot in those four exciting years about various academic disciplines, but most importantly, I obtained a greater understanding of my own capabilities. With the support of my friends and the challenges set down by some of the intellectual giants that emerged from Troy, I was able to push myself harder and accomplish far more than I could have ever imagined.

The next major step in my life involved a three-thousand mile journey to cold, cold city of Cambridge, Massachusetts. It was a step I had dreamed about taking since I was a child. Standing for the first time in the middle of Killian Court, taking in the glory of everything that was the Institute, I was blind to the gauntlet that lay before me. Soon enough, I would learn that the terrible stories about MIT were all true. And yet, I was able to do it all with a smile, thanks to my great friends at this university. To Shefali Oza and Laura Colon-Melendez, who always ended up laughing late into the night as we worked on torturously long problem sets; to Onsi Fakhouri, who was not only able to keep from defenestrating me during the year that we were Junior Lab partners, but ended up becoming one of the few people I could truly rely on; to Shankar Mukherji, Nasser Demir, and Joel Corbo, who somehow relieved my stress during the times at which it was least likely; to Elvio, John, Kelly, and Caroline, who in some manner are involved in virtually every one of my ridiculous stories about MIT; and to my Brothers at the Epsilon Theta Chapter of Sigma Nu Fraternity, who have filled my years at MIT with joyful memories; you have paved the road to my success. You are my war buddies, the ones who stuck by me in the face of seemingly insurmountable odds.

And then there are the teachers. From my summers at Caltech are Szabi Márka, John Zweizig, and Mark Scheel. From MIT are Bolek Wyslouch, Deepto Chakrabarty, Richard Yamamoto, Ulrich Becker, Krishna Rajagopal, and Scott Hughes. Though each of these people has had an immeasurable impact on my life, I wish especially to Krishna Rajagopal and Scott Hughes.

Krishna is the kind of professor that every student of physics should have. He is, without question, the best teacher I have ever had, and probably the best I will ever have. For every day I knew Krishna, my respect for him grew. Though he was and still is a brilliant practitioner of quantum field theory, his expertise spanned the whole of physics, from the interactions of elementary particles

to the structures of relativistic stars. He was an inspiration to his students, not only because of his impressive mastery of the subjects he taught, but also because of his humanity. He cared about his students, and in many ways, he was one of us. Krishna has indelibly shaped my image of what a physicist should be.

After putting up with me for nearly two years, Scott Hughes deserves to be awarded a Congressional Medal of Honor. I first met Scott in January 2002, just a week after he moved to MIT. Though he was still busy getting his new life in order, he somehow found time to set me up with an interesting and important project to work on that would eventually form the underpinnings of this thesis. But as much as I did for him, he did ten times more for me. For the duration of our collaboration, Scott provided much-needed guidance in academic and life matters, and was always extremely supportive and understanding of my other responsibilities. He did not try to put himself above me, but managed to achieve a near-perfect balance of friendliness and didacticism. His encouragement always came in the form of joyful excitement, not an iron fist, and for that I will always be thankful.

Finally, I wish to thank Joel Franklin, who carried ten times his weight and some of mine by quietly doing a lot of the background research in support of this thesis. For the first several months, this work was sputtering along at a snail's pace. But once Joel arrived and infused the project with his tremendous energy, things took off at light speed.<sup>1</sup> Without his help, this thesis would certainly still be in its infancy.

To these people, and to those I have failed to mention here, I owe my twenty years of accomplishment. I am humbled by their generosity and faith; they have all contributed in some substantial way to my journey. Now at the end of a major stage in my life, I anxiously await the opportunity to discover what lies ahead. But I will never forget what lay behind, the powerful confluence of forces that permitted me to achieve this fantastic success.

Akash Kansagra  
May 2004

---

<sup>1</sup>This being a thesis on general relativity, I could not resist the urge to say "light speed."

# Contents

<b>1</b>	<b>Introduction</b>	<b>13</b>
1.1	Geodesics and Integrals of Motion . . . . .	17
1.2	Integrals of Motion in Kerr Spacetime . . . . .	18
1.3	Perturbations to the Geodesic Trajectory . . . . .	20
1.3.1	Additional Forces . . . . .	20
1.3.2	Evolution of First Integrals of Degree $n = 1$ . . . . .	20
1.3.3	Evolution of First Integrals of Degree $n = 2$ . . . . .	21
1.3.4	Consequences . . . . .	22
1.4	Papapetrou Equations . . . . .	23
<b>2</b>	<b>Geodesic Integration</b>	<b>27</b>
2.1	Orbital Constants of Motion . . . . .	27
2.2	Geodesics in Schwarzschild Spacetime . . . . .	28
2.2.1	Radial Motion . . . . .	28
2.2.2	Angular Motion . . . . .	30
2.3	Geodesics in Kerr Spacetime . . . . .	31
2.3.1	Radial Motion . . . . .	31
2.3.2	Angular Motion . . . . .	32
2.4	Momentum Equations . . . . .	36
2.5	Mapping between Constants . . . . .	37
2.5.1	$(E, L_z, Q) \rightarrow (p, e, \iota)$ . . . . .	37
2.5.2	$(p, e, \iota) \rightarrow (E, L_z, Q)$ . . . . .	39
2.6	Finding the Least Stable Orbit . . . . .	40
2.7	Integration . . . . .	43
2.7.1	Incorporating Spin . . . . .	44
<b>3</b>	<b>Spin and Orbital Evolution</b>	<b>45</b>
3.1	Mathematical Basis of Spin . . . . .	45

3.2	Evolution of Orbital Constants . . . . .	46
3.2.1	Evolution of the Energy and Angular Momentum . . . . .	46
3.2.2	Evolution of the Carter Constant . . . . .	47
3.2.3	Evolution of the Spin Tensor . . . . .	48
3.3	Supplementary Equations . . . . .	49
3.3.1	Center of Mass Constraint . . . . .	49
3.3.2	Spin Magnitude . . . . .	50
3.4	Spin-Parallel Particle in the Equatorial Plane . . . . .	50
3.4.1	Orbital Evolution . . . . .	51
3.4.2	Analytic Integration . . . . .	52
<b>4</b>	<b>Results and Discussion</b> . . . . .	<b>55</b>
4.1	A Prefatory Word on Spin . . . . .	55
4.2	Code Validation . . . . .	55
4.2.1	Convergence . . . . .	56
4.2.2	Constrained Orbits . . . . .	56
4.2.3	Decoupled Orbits . . . . .	56
4.3	Example Orbits . . . . .	59
4.4	Spin Orientation and Energy Splitting . . . . .	59
4.4.1	Spin in the Polar Direction . . . . .	63
4.4.2	Spin in the Radial Direction . . . . .	63
4.4.3	Spin in the Azimuthal Direction . . . . .	63
4.5	Variation of Orbital Constants . . . . .	67
4.5.1	Amplitude of Variation . . . . .	67
4.5.2	Frequency Components . . . . .	67
4.6	Phase Space Volume . . . . .	70
4.6.1	Volume Growth with Spin . . . . .	71
4.6.2	Volume Growth with Semilatus Rectum . . . . .	71
4.7	Outlook . . . . .	71
4.7.1	Radiation Reaction Timescales . . . . .	71
4.7.2	Radiation Reaction versus Spin . . . . .	74
4.8	Outstanding Issues . . . . .	74

# List of Figures

1-1	The physical configuration of the binary system . . . . .	14
1-2	Boyer-Lindquist coordinate system . . . . .	16
2-1	The radial quasi-potential $R(r)$ for a typical stable orbit around a Kerr black hole .	33
2-2	Discrepancy between $\iota$ and $ \frac{\pi}{2} - \theta_{\max} $ . . . . .	36
2-3	The radial quasi-potential $R(r)$ for a marginally stable orbit around a Kerr black hole	41
2-4	The radial quasi-potential $R(r)$ for an unstable orbit around a Kerr black hole . . .	42
4-1	A typical spin-enhanced orbit along with the corresponding geodesic . . . . .	57
4-2	Time dependence of $S^2$ for constrained and unconstrained orbits . . . . .	58
4-3	Variation of $S^{r\phi}$ along an orbit decoupled from spin . . . . .	60
4-4	Variation of constants for typical spin-enhanced orbit . . . . .	61
4-5	A spin-enhanced orbit with large $S$ . . . . .	62
4-6	Radial position of the particle with $\vec{S}$ aligned in the polar direction . . . . .	64
4-7	Radial position of the particle with $\vec{S}$ aligned in the radial direction . . . . .	65
4-8	Radial position of the particle with $\vec{S}$ aligned in the azimuthal direction . . . . .	66
4-9	Linear dependence of $\sigma_p$ on $S$ . . . . .	68
4-10	Power spectrum of orbital parameters . . . . .	69
4-11	Dependence of phase space volume on $S$ . . . . .	72
4-12	Dependence of phase space volume on $p$ . . . . .	73



# List of Tables

4.1	Amplitude of variation of orbital constants for an orbit with $a = 0.5 M$ , $p = 7 M$ , $e = 0.7$ , and $\iota = 30^\circ$ . . . . .	67
4.2	Amplitude of variation of orbital constants for an orbit with $a = 0.9 M$ , $p = 10 M$ , $e = 0.2$ , and $\iota = 10^\circ$ . . . . .	70



# Chapter 1

## Introduction

For all its mathematical complexity, general relativity brings with it a certain conceptual simplicity. For example, one can understand certain gravitational interactions, such as the orbit of a simple particle<sup>1</sup> around a rotating (Kerr) black hole, in a language inspired by electromagnetic interactions.

We can use the intuition from this electromagnetic analogy to understand the motion of a *spinning* particle around a Kerr black hole (see Fig. 1-1), which resembles a magnetic dipole moving in an external electromagnetic field. Virtually all macroscopic astrophysical objects have some amount of spin, and so extending our knowledge of the dynamics of binary systems to include the effects of spin is an important and obvious step.

It is the aim of this thesis to examine the dynamics of compact binary systems influenced by the existence of spin on the smaller body. To make the problem more tractable, we work exclusively in the *extreme mass ratio* regime (the test particle limit); if the mass of the particle is  $m$  and the mass of the central black hole is  $M$ , we require that  $m \ll M$ . This constraint is satisfied by many real systems. For example, there has been gathering evidence suggesting the existence of supermassive black holes ( $10^6 - 10^9 M_\odot$ , where  $M_\odot$  is the mass of the Sun, equal to about  $2 \times 10^{30}$  kg) in galactic nuclei [1, 2, 3]. One expects that small compact objects ( $1 - 10 M_\odot$ ) from the surrounding stellar population will be captured by these black holes following many-body scattering interactions at a relatively high rate [4, 5], resulting in precisely the type of binary systems that meet the requirements of the extreme mass ratio approximation.

Operationally, the extreme mass ratio approximation is useful because it allows us to write the actual spacetime  $g_{\mu\nu}$  as the superposition of the “background” spacetime of the Kerr black hole and a linear perturbation,

$$g_{\mu\nu} = g_{\mu\nu}^{\text{Kerr}} + \delta g_{\mu\nu}^{\text{particle}}, \quad (1.1)$$

---

<sup>1</sup>By “particle,” we mean any sufficiently small object. The key physical characteristics attached to the notion of “sufficiently small” are that the small body does not appreciably distort the spacetime (i.e., it has small mass), and that the small body does not sustain significant tidal distortion (i.e., it has small radius).

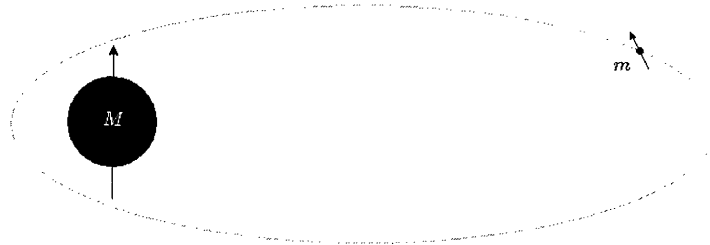


Figure 1-1: The configuration of the binary systems we will explore in this thesis. Both components of the binary are endowed with spin.

where  $g_{\mu\nu}^{\text{Kerr}}$  is the spacetime metric of the Kerr black hole and  $\delta g_{\mu\nu}^{\text{particle}}$  is the small contribution from the particle, including its spin (i.e.,  $\delta g_{\mu\nu}^{\text{particle}} \ll g_{\mu\nu}^{\text{Kerr}}$ ). The approximation allows us to replace the non-linear Einstein equations with linear ones and perform an analysis that is linearized about the black hole background.

Since  $g_{\mu\nu} \approx g_{\mu\nu}^{\text{Kerr}}$ , the geodesic paths which correspond to the allowed trajectories of spinning particles correspond approximately to those of a non-spinning particle in Kerr spacetime. This property is immensely useful to us; the geodesic orbit of a spinless particle in Kerr spacetime is completely integrable, thereby granting us the ability to reduce the equations which determine the geodesic to a set of ordinary differential equations which can be easily integrated to obtain the trajectory of the particle.<sup>2</sup>

However, we cannot just ignore the metric perturbation. Because  $g_{\mu\nu}$  does differ ever-so-slightly from  $g_{\mu\nu}^{\text{Kerr}}$ , we can expect that the geodesic trajectories of  $g_{\mu\nu}$  will gradually become distinct from those of  $g_{\mu\nu}^{\text{Kerr}}$ . But such differences can only be noticed over large intervals of time, after the accumulated effect of the perturbation on the orbit has become significant.

We can make this discussion somewhat more precise by jumping forward to a result that we discuss in detail later: orbits of non-spinning particles in Kerr spacetime are specified by a set of three constants,  $E$ ,  $L_z$ , and  $Q$ .<sup>3</sup> Because the trajectory of a spinning particle closely matches the trajectory of a non-spinning particle over short time intervals, we can specify the properties of the spin-enhanced trajectory near a time  $t_0$  with a set  $[E(t_0), L_z(t_0), Q(t_0)]$ . At some later time  $t_1$ , the trajectory most closely corresponds to a different set of constants  $[E(t_1), L_z(t_1), Q(t_1)]$ . We can construct the long-term behavior of the spin-enhanced trajectory by stitching together short segments of the trajectories of non-spinning particles, each corresponding to a possibly different point  $[E(t_i), L_z(t_i), Q(t_i)]$  in parameter space. In the limit of zero step size, the “constants” specifying the geodesic trajectory are allowed to vary continuously, giving rise to the full, spin-enhanced behavior

<sup>2</sup>Implicit here is the well-known fact that the trajectory of any small particle can be accurately approximated with a geodesic [6].

<sup>3</sup>In other words, the space of all possible Kerr orbits corresponds exactly to the space of allowed  $(E, L_z, Q)$ . Each point in this space corresponds to a unique geodesic, up to initial conditions.

which follows some orbit  $[E(t), L_z(t), Q(t)]$  through the space of Kerr geodesics. This is the essence of the perturbative approximation; we solve for the motion at each time step as though  $E$ ,  $L_z$ , and  $Q$  were constant, but then allow the constants to vary by a small amount. The important consideration in all of this is that the variation in the “constants” of motion must be small from step to step in order for the approximation to be accurate. We can automatically guarantee that  $E$ ,  $L_z$ , and  $Q$  satisfy this criterion by restricting our attention to small values of small-body spin.

We have before us a potentially fantastic development; if we are correct, we should be able to model spin-enhanced orbits using fairly simple modifications to the tools we use to study geodesic orbits.<sup>4</sup> It is the aim of the present work to determine how well we can model spin-enhanced trajectories within this perturbative scheme and paint a physical picture of the effect of spin on the motion of the test body.

This thesis is organized into four chapters. The remainder of Chapter 1 will focus on the theory of geodesic motion around Kerr black holes and weak perturbations to geodesic trajectories with the aim of developing the mathematical groundwork necessary to properly construct spin-enhanced orbits. Chapter 2 describes in detail the methods used to build a geodesic integrator and explains how the integrator can be expanded to include perturbative corrections. Chapter 3 contains derivations of the actual perturbative effects of spin, as well as the important special case of an equatorial, spin-parallel particle which clearly illustrates some of the effects of spin. In Chapter 4, we discuss the results obtained with our integrator. After performing a series of diagnostic tests, we explore the energy characteristics of various spin orientations. We then examine the spin-induced variation of orbital constants. Specifically, we study the scale of the variation, the timescales on which the variation occurs, and the “puffing out” of the orbit from a point to a finite volume in phase space.

Some comments on methodology and notation are in order. In maintaining sensitivity to fashion interests, we work in units of  $G = c = 1$ , but will restore these constants where it aids clarity. In these units, the mass of the sun is  $M_\odot = 4.92 \times 10^{-6}$  seconds, or 1.47 km. Following the convention of Carroll [10], we represent the components of relativistic four-vectors with a Greek superscript (e.g.,  $v^\mu$ ,  $\mu \in \{0, 1, 2, 3\}$ ). For reasons we will soon describe, we will never use  $\theta$  or  $\phi$  as four-vector indices. We can express  $\vec{v}$  in a basis  $e_\mu^\vec{v}$  as

$$\vec{v} = \sum_{\mu=0}^3 v^\mu e_\mu^\vec{v} = v^\mu e_\mu^\vec{v}, \quad (1.2)$$

but will loosely refer to  $\vec{v}$  as  $v^\mu$  in an implied spheroidal basis. Note also that we have adopted the Einstein summation convention by dropping the summation symbol in Eq. (1.2). This is standard

---

<sup>4</sup>Incidentally, many codes that include effects of gravitational radiation reaction do so in a similar manner. The celebrated Teukolsky-Sasaki-Nakamura formalism for calculating gravitational wave emission allows one to compute energy and angular momentum fluxes at infinity, which can be equated with energy and angular momentum loss rates from the system [7, 8, 9]. The energy and angular momentum of the orbit are then evolved in accordance with their loss through gravitational wave emission.

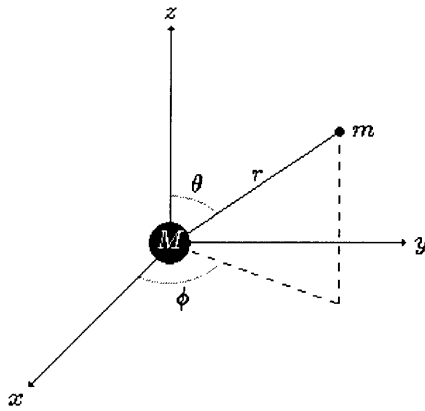


Figure 1-2: The spheroidal Boyer-Lindquist coordinate system used throughout this thesis. The  $x$ ,  $y$ , and  $z$  axes are defined as one would expect in “normal” spherical coordinates (i.e.,  $x = r \sin \theta \cos \phi$ ,  $y = r \sin \theta \sin \phi$ , and  $z = r \cos \theta$ ).

practice, and we will stick to it throughout this thesis.

We define the “0” component of  $\vec{v}$  as the time component, and the remaining three as the  $r$ ,  $\theta$ , and  $\phi$  components, respectively. These are the Boyer-Lindquist coordinates (see Fig. 1-2). Although it is appropriate to think of  $r$ , for example, as the radius, it should be recognized that the Boyer-Lindquist  $r$  only asymptotically approaches what most would normally think of as the radius. For clarity, we will refer to the individual components of  $\vec{v}$  by their corresponding coordinates:  $v^0 = v^t$ ,  $v^1 = v^r$ ,  $v^2 = v^\theta$ , and  $v^4 = v^\phi$ . It is for this reason that we avoid using  $\theta$  or  $\phi$  as four-vector indices—they already correspond to a particular four-vector component, and using them in any other way would cause confusion. In all cases, the meaning of vector components should be clear from the context.

The spacetime metric signature is  $(-, +, +, +)$ , so that the spacetime interval between two spacelike-separated events is positive. This sign choice for  $g_{\mu\nu}$  is standard for astrophysical work and is used in many popular texts (including Refs. [10] and [11]). Finally, round (square) brackets on tensor indices denote (anti-)symmetrization, so that

$$K_{(\mu\nu)} = \frac{1}{2} (K_{\mu\nu} + K_{\nu\mu}) \quad K_{[\mu\nu]} = \frac{1}{2} (K_{\mu\nu} - K_{\nu\mu}). \quad (1.3)$$

If more than two indices are enclosed within the brackets, the normalization factor is  $1/n!$  instead of  $1/2$ , where  $n$  is the number of enclosed indices.

It is also important to state that the orbits we generate in this thesis do not include the effects of gravitational radiation reaction. In Chapter 4, we will discuss the timescale on which radiation reaction operates, but again it is not included in the equations which govern the evolution of the orbiting particle.

## 1.1 Geodesics and Integrals of Motion

To understand the mathematical basis of geodesic motion, we must clearly define how we take time derivatives along the orbit of the particle. Differentiation along the orbit is achieved through covariant differentiation with respect to the proper time, denoted as  $D/D\tau$ . Physically, the covariant derivative corresponds to a directional time derivative along the tangent vector to the orbit (e.g., the velocity vector), and therefore,

$$\frac{D}{D\tau} = v^\mu \nabla_\mu, \quad (1.4)$$

where  $v^\mu$  is the four-velocity of the particle. The covariant time derivative of a quantity  $X$  is then

$$\dot{X} = v^\mu \nabla_\mu X,$$

where the overdot denotes  $D/D\tau$ . The covariant derivative  $\nabla_\mu$  is related to the familiar partial derivative through a set of connection coefficients  $\Gamma_{\mu\nu}^\sigma$ , the details of which can be found in any standard general relativity text (see, e.g., Refs. [10] and [11]).

Related to the four-velocity is the four-momentum,  $p^\mu$ . We can also define the specific four-momentum as  $u^\mu = p^\mu/m$  and require that it has norm

$$u^\mu u_\mu = -1. \quad (1.5)$$

The vector  $u^\mu$  is *not* necessarily parallel to  $v^\mu$  when one considers effects such as the existence of spin on the orbiting body. In the case that the small body has total spin  $\vec{S}$  with magnitude  $S$ , the difference  $u^\mu - v^\mu$  scales as  $S^2$ , which is of order  $m^2$ . In the extreme mass ratio regime, this discrepancy is small enough that it can be neglected. Any references to  $u^\mu$  and  $v^\mu$  can therefore be regarded as equivalent, except where explicitly stated.

A *geodesic* is a rather special trajectory corresponding to “free” motion. Such a trajectory satisfies

$$u^\mu \nabla_\mu p^\nu = \dot{p}^\nu = 0 \quad (1.6)$$

at all points. Equation (1.6) expresses the notion that a geodesic trajectory is one in which no forces act on the test particle.<sup>5</sup> Any forces on the particle will appear on the right hand side of Eq. (1.6) and will push the particle away from purely geodesic motion.<sup>6</sup>

With this information at hand we may compute the *integrals of motion*, which are scalar quan-

<sup>5</sup>Gravity is *not* a force in general relativity, but a geometric effect arising from the curvature of spacetime itself.

<sup>6</sup>For the sake of being explicit, we remind the reader that we are effectively modeling the geodesics of  $g_{\mu\nu}$  as geodesics in  $g_{\mu\nu}^{\text{Keir}}$  subject to forces corresponding to spin.

tities that remain fixed over the orbit. The existence of sufficiently many integrals of motion allows us to select particular geodesic trajectories out of the family of curves that satisfy Eq. (1.6).

We say that a spacetime admits a *first integral of degree  $n$*  if a scalar  $X$  satisfies

$$\dot{X} = u^\mu \nabla_\mu X = 0 \quad (1.7)$$

at all points on the orbit. The quantity  $X$  must be of the form

$$X = p_{\mu_1} \cdots p_{\mu_n} K^{\mu_1 \cdots \mu_n} \quad (1.8)$$

for some tensor  $K_{\mu_1 \cdots \mu_n}$ . The requirement that  $X$  remain constant along the geodesic is equivalent to *Killing's equation*,

$$\nabla_{(\mu} K_{\mu_1 \cdots \mu_n)} = 0. \quad (1.9)$$

If a spacetime admits as many integrals of motion as there are dimensions in the system, as is the case in Kerr spacetime, it is completely integrable.

## 1.2 Integrals of Motion in Kerr Spacetime

Much of our work in this thesis centers around the constants which specify orbits in Kerr spacetimes. As such, it is of much theoretical and practical value to determine the integrals of motion in the special case of orbits around a Kerr black hole. It turns out that we can find three such integrals of motion, corresponding to the total energy  $E$ , the  $z$  angular momentum  $L_z$ , and the so-called Carter constant  $Q$  of the orbiting particle. In fact, the mass  $m$  of the particle constitutes a fourth integral of motion, but we do not typically think of the mass as an interesting constant. Because there are four integrals of motion, the problem of a particle moving in a Kerr spacetime is completely integrable.

The Killing vector field corresponding to  $E$  is  $T^\mu = (-1, 0, 0, 0)$ . The minus sign is a conventional choice which guarantees that the energy is positive. As in classical mechanics, conservation of energy arises from symmetry under time translation. Following Eq. (1.8), we can define  $E$  as

$$E = p_\mu T^\mu = -p_t, \quad (1.10)$$

since the only non-zero component of  $T^\mu$  is  $T^t$ .

As with energy, the conservation of  $z$  angular momentum originates from a symmetry of the Kerr metric, but its symmetry is a spatial one. Specifically, a constant  $L_z$  arises from symmetry under

rotations in the  $\phi$  coordinate and corresponds to a Killing vector  $\Phi^\mu = (0, 0, 0, 1)$ . Accordingly,

$$L_z = p_\mu \Phi^\mu = p_\phi. \quad (1.11)$$

Note that the subscript  $z$  in  $L_z$  is a latin character, and is therefore *not* an index. Instead, the  $z$  simply indicates that the angular momentum is measured with respect to the  $z$  axis.

The Carter constant is more complicated, since it arises from a Killing tensor of rank  $n = 2$  instead of a simple vector. Carroll [10] and Chandrasekhar [6] indicate that the Killing tensor corresponding to the Carter constant  $K$  can be written as

$$K_{\mu\nu} = \Sigma l_{(\mu} n_{\nu)} + r^2 g_{\mu\nu}, \quad (1.12)$$

with

$$l_\mu = \left( 1, -\frac{\Sigma}{\Delta}, 0, -a \sin^2 \theta \right) \quad (1.13)$$

$$n_\mu = \left( \frac{\Delta}{\Sigma}, 1, 0, -\frac{a\Delta \sin^2 \theta}{\Sigma} \right) \quad (1.14)$$

$$\Sigma = r^2 + a^2 \cos^2 \theta \quad (1.15)$$

$$\Delta = r^2 - 2Mr + a^2, \quad (1.16)$$

where  $M$  is the mass of the black hole,  $a$  is the Kerr spin parameter defined by  $a = |\vec{S}|/M$  with  $\vec{S}$  representing the angular momentum of the black hole (distinct from the small body spin vector  $\vec{S}$ ),  $r$  is the Boyer-Lindquist radius, and  $\theta$  is the angle between  $\vec{S}$  and the radius vector to the particle. The Carter Killing tensor is clearly much more elaborate than the Killing tensors for energy or angular momentum.

We obtain the constant  $K$  as expected,

$$\begin{aligned} K &= p^\mu p^\nu K_{\mu\nu} \\ &= \Sigma^2 \left( \frac{d\theta}{d\tau} \right)^2 + \cos^2 \theta [a^2 (1 - E^2) + L_z^2 \csc^2 \theta] + (aE - L_z)^2. \end{aligned} \quad (1.17)$$

For our purposes, it is more useful to define a constant  $Q$ , related to  $K$  by

$$\begin{aligned} Q &= K - (aE - L_z)^2 \\ &= \Sigma^2 \left( \frac{d\theta}{d\tau} \right)^2 + \cos^2 \theta [a^2 (1 - E^2) + L_z^2 \csc^2 \theta]. \end{aligned} \quad (1.18)$$

When the black hole spin is zero,  $Q$  has the nice property of reducing to  $L_{\text{perp}}^2$ , where  $L_{\text{perp}}$  is the magnitude of the angular momentum projected into the orbital/equatorial plane. Such a notion

does not make perfect sense for a rotating black hole, but the intuition it provides remains useful. Any further references to the Carter constant may be regarded as references to  $Q$ .

## 1.3 Perturbations to the Geodesic Trajectory

### 1.3.1 Additional Forces

When we want to include additional physical effects into the motion of a particle around a black hole, we must supplement Eq. (1.6) with additional force terms, so that

$$u^\nu \nabla_\nu p^\mu = \dot{p}^\mu = f^\mu. \quad (1.19)$$

The four-vector  $f^\mu$  encodes all of the “extra” forces that affect the small body. These extra forces might include spin, gravitational wave emission, tidal forces, self-gravity, or anything else; the additional force terms are completely generic. As a consequence, our results in the coming sections hold for any forces that can be described by  $f^\mu$ . One can, in principle, use the coming results to study any binary system.

The important effect of  $f^\mu$  is that the traditional constants of motion—in the case of a Kerr black hole, these are the energy, angular momentum, and Carter constant—are no longer exactly constant (though we continue to refer to them as “the orbital constants” for lack of a better name), but vary at a rate proportional to  $f^\mu$ . The perturbative force causes the orbit to follow some trajectory through  $(E, L_z, Q)$  space. In the absence of such perturbing forces, the orbit would correspond to a single point in  $(E, L_z, Q)$  space.

### 1.3.2 Evolution of First Integrals of Degree $n = 1$

For an arbitrary Killing vector  $\vec{K}$  with  $n = 1$ , Eqs. (1.8) and (1.9) yield

$$X = p^\mu K_\mu \quad (1.20)$$

$$\nabla_{(\mu} K_{\nu)} = 0 \quad (1.21)$$

From this we can easily compute  $\dot{X}$ :

$$\begin{aligned} \dot{X} = u^\mu \nabla_\mu X &= u^\mu (p^\nu \nabla_\mu K_\nu + K_\nu \nabla_\mu p^\nu) \\ &= \frac{1}{m} (p^\mu p^\nu \nabla_\mu K_\nu) + K_\nu u^\mu \nabla_\mu p^\nu \\ &= \frac{1}{m} (p^\mu p^\nu \nabla_\mu K_\nu) + K_\nu f^\nu \end{aligned} \quad (1.22)$$

$$= \frac{1}{m} (p^\nu p^\mu \nabla_\nu K_\mu) + K_\nu f^\nu, \quad (1.23)$$

where in Eq. (1.23) we have switched the indices in the first term of Eq. (1.22). If we add Eqs. (1.22) and (1.23) together, we find that

$$2\dot{X} = \frac{2}{m} p^\mu p^\nu \underbrace{\nabla_{(\nu} K_{\mu)}}_0 + 2K_\nu f^\nu, \quad (1.24)$$

or,

$$\dot{X} = u^\mu \nabla_\mu X = K_\mu f^\mu = K^\mu f_\mu. \quad (1.25)$$

We can use this result to obtain specific evolution equations for  $E$  and  $L_z$  in terms of  $f^\mu$  by substituting the appropriate  $K^\mu$ . By definition, the Killing vectors for  $E$  and  $L_z$  are  $\vec{T} = -\vec{e}_t$  and  $\vec{\Phi} = \vec{e}_\phi$ , respectively, so

$$\dot{E} = T^\mu f_\mu = -f_t \quad (1.26)$$

$$\dot{L}_z = \Phi^\mu f_\mu = f_\phi. \quad (1.27)$$

These equations govern the evolution of  $E$  and  $L_z$  along the orbital path. By setting  $f^\mu = 0$ , we recover  $\dot{E} = \dot{L}_z = 0$  as required.

### 1.3.3 Evolution of First Integrals of Degree $n = 2$

Equations (1.8) and (1.9) with  $n = 2$  yield

$$X = p^\mu p^\nu K_{\mu\nu} \quad (1.28)$$

$$\nabla_{(\mu} K_{\nu\sigma)} = 0. \quad (1.29)$$

As usual, we must compute  $\dot{X} = u^\mu \nabla_\mu X$ , from which we find

$$\begin{aligned} u^\mu \nabla_\mu X &= \frac{1}{m} (p^\mu p^\nu p^\sigma \nabla_\mu K_{\nu\sigma}) + (p^\mu p^\sigma \nabla_\mu p^\nu + p^\mu p^\nu \nabla_\mu p^\sigma) K_{\nu\sigma} \\ &= \frac{1}{m} [p^\mu p^\nu p^\sigma \nabla_\mu K_{\nu\sigma} + (p^\sigma f^\nu + p^\nu f^\sigma) K_{\nu\sigma}] \end{aligned} \quad (1.30)$$

If we cyclically permute the indices in the first term of Eq. (1.30), we obtain a set of six equations which we sum to obtain

$$6u^\mu \nabla_\mu X = \frac{6}{m} p^\sigma p^\mu p^\nu \underbrace{\nabla_{(\sigma} K_{\mu\nu)}}_0 + 6(f^\mu p^\nu + f^\nu p^\mu) K_{\mu\nu},$$

or,

$$\begin{aligned}\dot{X} = u^\mu \nabla_\mu X &= (p^\mu f^\nu + p^\nu f^\mu) K_{\mu\nu} \\ &= 2p^{(\mu} f^{\nu)} K_{\mu\nu}.\end{aligned}\tag{1.31}$$

In the special case that  $K_{\mu\nu}$  is symmetric, i.e.  $K_{\mu\nu} = K_{\nu\mu}$ , we can further simply this result to remove explicit symmetrization

$$\dot{X} = 2p^\mu f^\nu K_{\mu\nu}.\tag{1.32}$$

This result allows us to determine the evolution of the Carter constant. Since  $Q = K - (aE - L_z)^2$  and  $\dot{K} = 2p^\mu f^\nu K_{\mu\nu}$  with  $K_{\mu\nu}$  being the symmetric Carter Killing tensor, we find

$$\begin{aligned}\dot{Q} &= \dot{K} - 2(aE - L_z)(a\dot{E} - \dot{L}_z) \\ &= 2p_\mu f_\nu [K^{\mu\nu} - (\Phi^\mu - aT^\mu)(\Phi^\nu - aT^\nu)].\end{aligned}\tag{1.33}$$

This evolution equation predicts that  $\dot{Q} = 0$  if  $f^\mu = 0$ , exactly as we require. Equations (1.26), (1.27), and (1.33) together encode the evolution of all three orbital constants  $E$ ,  $L_z$ , and  $Q$  under the influence of an arbitrary force.

### 1.3.4 Consequences

The evolution equations for the orbital constants scale as  $f^\mu$ . In many important cases,  $f^\mu$  is small, and the *variation of the constants is small*. This is a critical observation, and it practically screams for a perturbative approach. There are already a wide variety of tools for studying orbits in which the constants are fixed, and it is a simple and straightforward matter to generalize these tools to include other forces by “freeing” the orbital constants and keeping everything else the same. One must not forget, however, that  $f^\mu$  might itself evolve, if for no other reason than that the evolution of the orbital “constants” will change the orbit. It is therefore necessary, in general, to include evolution equations not just for the coordinates and the constants, but also  $f^\mu$ .

Our equations thus far have purposefully been written in an extremely general way, and for good reason. Given almost any physically reasonable  $f^\mu$ , provided it is sufficiently small, one can understand the motion of *any* object subject to forces. The only statement we have made that is even slightly sneaky is that  $v^\mu$  and  $u^\mu$  can be regarded as parallel. In fact, this is true to very good accuracy for the case of small body spin since the difference scales as  $S^2$ , but remains true for virtually every effect we can imagine in the test particle limit.<sup>7</sup> All we have said is that if  $f^\mu$  is

---

<sup>7</sup>As a point of fact, dropping  $S^2$  terms is a *requirement* of the approach we use. Regardless of whether these terms are physically relevant, the only way we can sensibly use the Kerr spacetime as a background is to ensure that  $p^\mu$  and

some supplemental force—it does not matter what it corresponds to—then the equations governing the evolution of  $E$ ,  $L_z$ , and  $Q$  can be obtained by Eqs. (1.26), (1.27), and (1.33). In other words, this scheme can be used to study a wide array of forces. For a simple and interesting example, one might consider the electromagnetic force on a test particle with a small amount of charge  $q$ , which has the relatively simple expression

$$f^\nu = qv_\mu F^{\mu\nu}, \quad (1.34)$$

where  $F^{\mu\nu}$  is the electromagnetic field strength tensor [10]. For the remainder of this thesis, however, we will depart from our general approach and specialize our study of geodesic perturbations to the case of small body spin.

## 1.4 Papapetrou Equations

A geodesic trajectory presupposes that the small particle can be described perfectly as a mass monopole. This is not always sufficient. Small body spin introduces higher-order mass terms to the equations of motion. The resulting force on the particle due to the coupling of small body spin to the spacetime curvature is very similar in nature to the force that acts on a magnetic dipole in the presence of an external electromagnetic field.

To obtain the mass dipole effects, one must turn to the Papapetrou equations [12], which have since been recast into a more useful form by Dixon [13].<sup>8</sup> In their purest form, the Papapetrou equations can be written as a set of three tensor equations,

$$\frac{dx^\mu}{d\tau} = v^\mu \quad (1.35)$$

$$\frac{Dp^\mu}{D\tau} = -\frac{1}{2}R^\mu{}_{\nu\alpha\beta}v^\nu S^{\alpha\beta} \quad (1.36)$$

$$\frac{DS^{\mu\nu}}{D\tau} = 2p^{[\mu}v^{\nu]}, \quad (1.37)$$

where  $R^\mu{}_{\nu\alpha\beta}$  is the Riemann curvature tensor and  $S^{\mu\nu}$  is the antisymmetric spin tensor [14]. These equations are usually supplemented with the *center of mass constraint*,

$$p_\mu S^{\mu\nu} = 0, \quad (1.38)$$

which designates the position of the center of the orbiting particle [14]. One can also write down an

---

$v^\mu$  are parallel, which is true only to order  $S$ . The derivation of the Kerr geodesics assumes that the two vectors are parallel, and hence it must stay that way.

<sup>8</sup>The Papapetrou equations do not provide information about the quadrupole terms that cause tidal disruption. Quadrupole effects (and potentially even higher order effects) are important in certain cases, but not for small compact bodies. We are concerned here with the capture of black holes, neutron stars, or other “particles,” and so this limit is useful.

equation for spin conservation;

$$\frac{1}{2}S_{\mu\nu}S^{\mu\nu} = S^2, \quad (1.39)$$

where the constant  $S$  corresponds to the magnitude of the spin on the small body.<sup>9</sup> One typically enforces the center of mass constraint equation because the existence of spin affects the formal integrability of the system. As written, these equations are valid *along geodesics*; we will reconsider this issue in greater depth in Chapter 3.

As far as units are concerned, the important point to be made is that  $S$  is measured in terms of  $mM$ . Hartl discusses the aftermath of previous confusion about this issue, which generated a relatively widespread belief that chaos could easily occur for spinning particles, in Ref. [14]. In these units, we can think of  $S$  for a maximally spinning particle as the mass ratio itself. In particular, the spin magnitude for a maximally spinning object is  $S = m^2$ , from which it follows that  $S/mM = m/M$ .

The Papapetrou equations deserve a second look. Equation (1.35) corresponds to the definition of the four-velocity, and it does not tell us anything that is particularly interesting. But Eqs. (1.36) and (1.37) are new. In fact, if we remember our definition of the local force  $f^\mu = Dp^\mu/D\tau$ , we can read off directly from Eq. (1.36) that

$$f^\mu = -\frac{1}{2}R^\mu_{\nu\alpha\beta}v^\nu S^{\alpha\beta}. \quad (1.40)$$

This is precisely the force experienced by the test particle.

While Eq. (1.36) encodes the force on the particle and the evolution of orbital constants, Eq. (1.37) encodes the evolution of the spin tensor  $S^{\mu\nu}$  itself—and by association,  $f^\mu$  as well. In effect, it contains the physics governing the free precession of a gyroscope in curved spacetime. As we alluded to before, Eq. (1.37) is not precisely zero, since the four-momentum  $p^\mu$  and the four-velocity  $v^\mu$  are not strictly parallel—the difference is of order  $S^2$ —when one includes small body spin. But since  $S$  is small, we can ignore higher orders of  $S$  and regard  $v^\mu$  and  $p^\mu$  as parallel. We can therefore restate the Papapetrou equations as they appear in our analysis,

$$\frac{dx^\mu}{d\tau} = v^\mu \quad (1.41)$$

$$\frac{Dp_\mu}{D\tau} = -\frac{1}{2}R_{\mu\nu\alpha\beta}v^\nu S^{\alpha\beta} \quad (1.42)$$

$$\frac{DS^{\mu\nu}}{D\tau} = 0. \quad (1.43)$$

Equation (1.42) can be used to calculate  $\dot{E}$ ,  $\dot{L}_z$ , and  $\dot{Q}$  (see Chapter 3). As such, this final set

---

<sup>9</sup>Note that the conservation of  $S^2$  is not a constraint, but a definition. The center of mass condition *is* a constraint, however, since  $p_\mu S^{\mu\nu} = 0$  cannot be derived from the Papapetrou equations.

of equations provides all the information we need to enable a standard Kerr geodesic integrator to evolve the orbital constants in a manner consistent with the existence of small body spin.



## Chapter 2

# Geodesic Integration

In this chapter we consider the motion of a small particle around a Kerr black hole. The trajectories of small particles can be very accurately approximated as geodesics [6]. The equations which determine the geodesics are a set of analytic ordinary differential equations which can be integrated with relative ease on a computer.

Such a numerical implementation is not trivial, however, and it is necessary to describe in some detail the techniques which we use to generate small particle orbits. Portions of this discussion are drawn from Refs. [15] and [16]. Along the way, we will explain our own simple method of incorporating the effects of spin.

### 2.1 Orbital Constants of Motion

Every orbit around a black hole is specified up to initial conditions by the energy  $E$ , the  $z$  angular momentum  $L_z$ , and the Carter constant  $Q$ . The energy and the angular momentum are both proportional to  $m$ , whereas the Carter constant is of order  $m^2$ . For the sake of numerical and theoretical simplicity, we will eliminate  $m$  from our equations and use the appropriately normalized forms of  $E$ ,  $L_z$ , and  $Q$ . In particular, we will redefine (for this chapter only) the orbital constants such that

$$E = \frac{E^{\text{usual}}}{m} \quad L_z = \frac{L_z^{\text{usual}}}{m} \quad Q = \frac{Q^{\text{usual}}}{m^2}, \quad (2.1)$$

which amounts to setting  $m = 1$ . Using these “new” constants ensures that factors of  $m$  are completely absent from the equations of motion. However,  $L_z$  and  $Q$  still involve factors of  $M$ , but both always appear in proper combination with other dimensionful quantities in the equations of motion. We maintain dimensions in the written equations for the sake of clarity, but casting the equations in completely dimensionless form is as simple as setting  $M = 1$ .

All bound orbits have  $E < 1$ , due to the fact that the energy of the particle is given by the rest energy  $mc^2 = 1$  plus a negative gravitational binding energy. (We never consider the case of unbound orbits, for which  $E \geq 1$ , although it appears straightforward to do so.) The angular momentum  $L_z$  is defined relative to the black hole's spin axis. The Carter constant corresponds roughly to the norm of the “rest” of the angular momentum,  $L_x^2 + L_y^2$ . Though the equality between  $Q$  and  $L_x^2 + L_y^2$  is not exact in Kerr spacetime, the insight provided by the approximate correspondence remains useful.

Following standard practice, we use the total black hole spin  $\vec{S}$  to define a new constant  $a = |\vec{S}|/M$  with units of  $M$ . The parameter  $a$ , called the “Kerr spin parameter,” can assume any value in the range  $0 \leq a \leq M$ . The case  $a = 0$  corresponds to a Schwarzschild black hole, and the case  $a = M$  is referred to as a “maximally spinning” black hole. Since  $\vec{S}$  does not change,  $a$  is fixed permanently.

## 2.2 Geodesics in Schwarzschild Spacetime

In terms of Boyer-Lindquist coordinates  $(t, r, \theta, \phi)$ , the geodesics of a Schwarzschild black hole are given by the following equations [11]:

$$\left(\frac{dr}{d\tau}\right)^2 = E^2 - \left(1 - \frac{2M}{r}\right) \left(1 + \frac{L_z^2 + Q}{r^2}\right) \quad (2.2)$$

$$\left(\frac{d\theta}{d\tau}\right)^2 = \frac{Q - L_z^2 \cot^2 \theta}{r^4} \quad (2.3)$$

$$\left(\frac{d\phi}{d\tau}\right) = \frac{L_z \csc^2 \theta}{r^2} \quad (2.4)$$

$$\left(\frac{dt}{d\tau}\right) = \frac{E}{1 - 2M/r} \quad (2.5)$$

These equations specify the position of the orbiting particle up to initial conditions. Note that the time  $t$  equals the time as measured on clocks far from the black hole. Thus, Eq. (2.5) allows us express the evolution of the orbit as seen by distant observers by recasting the equations of motions in terms of  $t$  instead of  $\tau$ .

### 2.2.1 Radial Motion

There is a complication in Eq. (2.2), owing to the fact that the radial derivative appears quadratically. We cannot simply take the square root of the equation, since doing so would prevent us from determining the sign of the radial velocity, resulting in an inability to distinguish an infalling particle from an outfalling one. We can get around this problem by parameterizing  $r$  in terms of another

variable whose derivative is always positive. The parameterization we use is elliptic;

$$r = \frac{p}{1 + e \cos \psi}, \quad (2.6)$$

with  $p$  and  $e$  representing two of the three quantities we use to identify orbits *geometrically*.<sup>1</sup> This parameterization will allow us to encode the oscillation of  $r$  in the *monotonic* growth of  $\psi$ . The monotonicity of the evolution is key; it guarantees we can take the square root of  $d\psi/d\tau$  without worrying about its sign. Using Eq. (2.6), we find that

$$\frac{dr}{d\tau} = \frac{pe \sin \psi}{(1 + e \cos \psi)^2} \frac{d\psi}{d\tau} = \frac{r^2 e \sin \psi}{p} \frac{d\psi}{d\tau}. \quad (2.7)$$

As expected,  $dr/d\tau$  is zero for a perfectly circular ( $e = 0$ ) orbit. We will use Eq. (2.7) shortly.

Returning to Eq. (2.2), we have that

$$\left(\frac{dr}{d\tau}\right)^2 = \frac{E^2 r^4 - r^4 (1 - 2M/r) [1 + (L_z^2 + Q)/r^2]}{r^4} \quad (2.8)$$

$$= \frac{(E^2 - 1) r^3 + 2M r^2 - (L_z^2 + Q) r + 2M (L_z^2 + Q)}{r^3} \quad (2.9)$$

$$= (E^2 - 1) \frac{r^3 + c_2 r^2 + c_1 r + c_0}{r^3}, \quad (2.10)$$

with

$$c_2 = \frac{2M}{E^2 - 1} \quad (2.11)$$

$$c_1 = -\frac{L_z^2 + Q}{E^2 - 1} \quad (2.12)$$

$$c_0 = \frac{2M (L_z^2 + Q)}{E^2 - 1}. \quad (2.13)$$

We can factor Eq. (2.10) to obtain

$$\left(\frac{dr}{d\tau}\right)^2 = (E^2 - 1) \frac{(r - r_3)(r - r_2)(r - r_1)}{r^3}. \quad (2.14)$$

This equation is far more instructive than Eq. (2.10) since two of the roots  $r_3$ ,  $r_2$ , and  $r_1$  correspond to turning points of the motion. We define the ordering of these roots to satisfy  $r_1 < r_2 < r_3$ , in which case  $r_3$  corresponds to the largest distance between the orbiting particle and the central body (the apastron distance) and  $r_2$  similarly designates the smallest distance between the bodies (the periastron distance).<sup>2</sup> The roots  $r_3$  and  $r_2$  thus define the boundaries of the radial motion. The

<sup>1</sup>This parameterization defines an ellipse in  $r, \psi$  space. In this context,  $p$  is the *semilatus rectum*, and  $e$  is the *eccentricity*. The eccentricity  $e$  must fall between 0 and 1, and the semilatus rectum  $p$  must be larger than some cutoff value, as we will discuss in Section 2.6. In the literature,  $\psi$  is often referred to as the *true anomaly*.

<sup>2</sup>It is common to write  $r_a$  and  $r_p$  in place of  $r_3$  and  $r_2$ , respectively, to reflect the fact that they correspond to

inner root  $r_1$  does not correspond to anything physical.

From Eq. (2.6), we know that the extremal values of  $r$  occur at

$$r_3 = \frac{p}{1-e} \quad r_2 = \frac{p}{1+e}. \quad (2.15)$$

By making these substitutions in Eq. (2.14) and with the help of Eq. (2.7), we obtain an expression for  $d\psi/d\tau$ :

$$\begin{aligned} \frac{d\psi}{d\tau} &= \underbrace{\left(\frac{1+e\cos\psi}{p}\right)^2}_{1/r} \sqrt{\frac{(1-E^2)p(p-r_1-er_1\cos\psi)}{1-e^2}} \\ &= \frac{p}{r^2} \sqrt{\frac{(1-E^2)(1-r_1/r)}{1-e^2}}. \end{aligned} \quad (2.16)$$

We can compute the square root without fear of sign ambiguities, since  $d\psi/d\tau$  is always greater than zero.

## 2.2.2 Angular Motion

In Eq. (2.3), it appears as though we may have to define another parameterization. In principle, this is true as long as we wish to unambiguously compute the square root of Eq. (2.3) to obtain an equation for  $d\theta/d\tau$ . In practice, however, matters are greatly simplified by the spherical symmetry of the Schwarzschild metric. In particular, we are free to choose the orbital plane to coincide with the equatorial plane, since *every* plane through the center of the black hole is equivalent.<sup>3</sup> As the equatorial plane is conventionally defined by  $\theta = \pi/2$ , the right hand side of Eq. (2.3) vanishes. A more physical way of thinking about this issue involves the realization that the gravitational potential is independent of  $\theta$ , and therefore, gravity cannot affect the  $\theta$  motion of the particle.<sup>4</sup>

The azimuthal derivative is simple enough to integrate that we need not discuss it in great detail. However, we can say that Eq. (2.4) is the Boyer-Lindquist equivalent of Kepler's Second Law. Equations (2.4), (2.5), and (2.16) together represent the equations of motion around a Schwarzschild black hole.

---

apastron and periastron. Other equivalent terms are sometimes used in place of apastron and periastron; Sigurdsson and Rees use "apbothron" and "peribothron" (see Ref. [4]), whereas Kip Thorne prefers "apholion" and "periholion."

<sup>3</sup>This also implies that we can always define a Schwarzschild geodesic with  $Q = 0$ .

<sup>4</sup>It should be noted that, mathematically speaking, one can very well start the particle off at  $\theta \neq \pi/2$ . In a polar orbit, for example,  $\theta$  most definitely changes with time. The insight we wish to have imparted here is that one *can* fix  $\theta = \pi/2$  if desired.

## 2.3 Geodesics in Kerr Spacetime

The geodesic equations in Kerr spacetime are similar to those in the Schwarzschild case, but they additionally involve the spin parameter  $a$ . We can write the geodesic equations for Kerr spacetime as follows [11]:

$$\Sigma^2 \left( \frac{dr}{d\tau} \right)^2 = [E(r^2 + a^2) - aL_z]^2 - \Delta [r^2 + (L_z - aE)^2 + Q] = R(r) \quad (2.17)$$

$$\Sigma^2 \left( \frac{d\theta}{d\tau} \right)^2 = Q - L_z^2 \cot^2 \theta - a^2 (1 - E^2) \cos^2 \theta = \Theta(\theta) \quad (2.18)$$

$$\Sigma \left( \frac{d\phi}{d\tau} \right) = \frac{2aMrE - a^2 L_z}{\Delta} + L_z \csc^2 \theta \quad (2.19)$$

$$\Sigma \left( \frac{dt}{d\tau} \right) = \frac{\gamma E - 2aMrL_z}{\Delta} \quad (2.20)$$

with  $\Sigma = r^2 + a^2 \cos^2 \theta$ ,  $\Delta = r^2 - 2Mr + a^2$ , and  $\gamma = (r^2 + a^2)^2 - a^2 \Delta \sin^2 \theta$ . Note that the existence of spin on the black hole has destroyed the spherical symmetry of the system, thereby eliminating the freedom we enjoyed in the Schwarzschild case to identify the orbital plane with the equatorial plane. The azimuthal symmetry which characterizes the Kerr solution is of a lower order than the spherical symmetry of the Schwarzschild metric and requires an additional constant to parameterize the motion. Whereas Schwarzschild geodesics can be specified by a set  $(E, L_z)$  or  $(p, e)$ ,<sup>5</sup> we will need to specify Kerr geodesics by  $(E, L_z, Q)$  or  $(p, e, \iota)$ . We already know the meaning of  $E$ ,  $L_z$ , and  $Q$ , as well as the interpretation of  $p$  and  $e$  as the semilatus rectum and eccentricity, respectively. What is left is the inclination angle  $\iota$ , which is defined by  $Q = L_z^2 \tan^2 \iota$  and agrees closely with the maximum polar angle between the equatorial plane and the particle position. We will discuss this in more detail in Sec. 2.3.2.

Equations (2.19) and (2.20) are already in a usable form. However, Eqs. (2.17) and (2.18) must be linearized. In the case of Eq. (2.17), we can accomplish this in essentially the same way we did for the Schwarzschild black hole, again using  $r = p / (1 + e \cos \psi)$ . For Eq. (2.18), we must invent a new change of variables.

### 2.3.1 Radial Motion

Expanding Eq. (2.17) in powers of  $r$ , we get

$$\begin{aligned} \Sigma^2 \left( \frac{dr}{d\tau} \right)^2 &= (E^2 - 1) r^4 + 2Mr^3 + [a^2 (E^2 - 1) - L_z^2 - Q] r^2 \\ &\quad + 2M [(Ea - L_z)^2 + Q] r - Qa^2 \end{aligned} \quad (2.21)$$

$$= (E^2 - 1) (r^4 + c_3 r^3 + c_2 r^2 + c_1 r + c_0), \quad (2.22)$$

---

<sup>5</sup>Since  $Q$  can always be set to zero for Schwarzschild orbits.

with

$$c_3 = \frac{2M}{E^2 - 1} \quad (2.23)$$

$$c_2 = a^2 - \frac{L_z^2 + Q}{E^2 - 1} \quad (2.24)$$

$$c_1 = \frac{2M \left[ (Ea - L_z)^2 + Q \right]}{E^2 - 1} \quad (2.25)$$

$$c_0 = -\frac{Qa^2}{E^2 - 1}. \quad (2.26)$$

These coefficients correspond to those for the Schwarzschild case if we set  $a$  and  $Q$  to zero.

For the Kerr black hole, the polynomial we must factorize is quartic. The  $\Sigma^2$  term does not contribute any interesting roots, so finding the roots of the right-hand side of Eq. (2.22) is equivalent to determining the turning points of the motion (see Fig. 2-1). Rewriting Eq. (2.22) in factored form as

$$\left( \frac{dr}{d\tau} \right)^2 = \frac{(E^2 - 1)(r - r_3)(r - r_2)(r - r_1)(r - r_0)}{\Sigma^2}, \quad (2.27)$$

with  $r_0 < r_1 < r_2 < r_3$ , we can use Eq. (2.7) and substitute  $r = p/(1 + e \cos \psi)$ ,  $r_3 = p/(1 - e)$ , and  $r_2 = p/(1 + e)$  to generate

$$\frac{d\psi}{d\tau} = \frac{p}{\Sigma} \sqrt{\frac{(1 - E^2)(1 - r_0/r)(1 - r_1/r)}{1 - e^2}} \quad (2.28)$$

This equation governs the radial motion of a particle around a Kerr black hole. It reduces to Eq. (2.16) when  $r_0 = 0$ .

### 2.3.2 Angular Motion

The equation for  $d\phi/d\tau$ , though considerably more complicated than in the Schwarzschild case, is just as easy to integrate since it appears linearly. Computing the polar motion, however, is more subtle; the derivative  $d\theta/d\tau$  appears quadratically, and we do not have any tricks that will allow us to avoid this complication in Kerr spacetime.

To parameterize  $\theta$ , we follow the prescription offered by Wilkins and set  $z = \cos^2 \theta$  [17]. In this

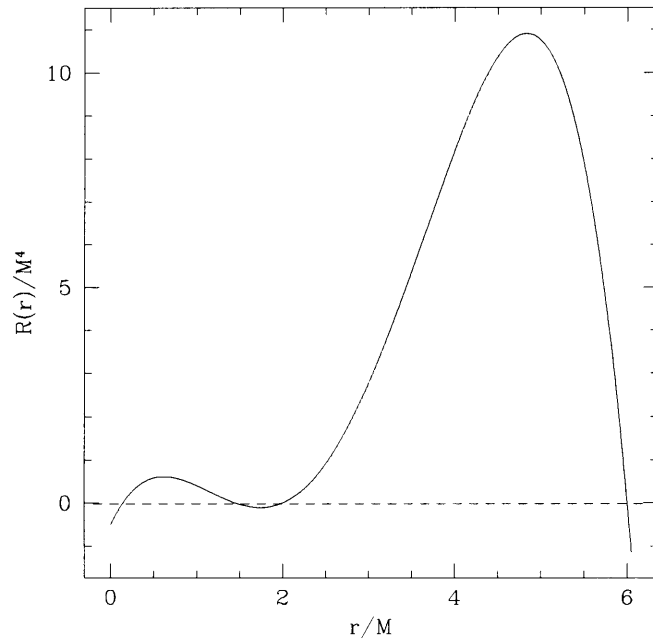


Figure 2-1: The radial quasi-potential  $R(r)$  for a stable orbit around a black hole with  $a = 0.95M$ . The orbit has  $p = 3M$ ,  $e = 0.5$ ,  $\iota = 20^\circ$ . Apastron occurs at  $r_3 = 6M$  and periastron occurs at  $r_2 = 2M$ ; these are the two outermost roots in the diagram. The other two roots  $r_1$  and  $r_0$  are inaccessible by orbiting particles. Figure adapted from Ref. [15].

case, we have

$$\begin{aligned}
\left(\frac{d\theta}{d\tau}\right)^2 &= \frac{Q - z [Q + L_z^2 + a^2 (1 - E^2)] + z^2 a^2 (1 - E^2)}{\Sigma^2 (1 - z)} \\
&= \beta \frac{Q/\beta - z \left(\frac{\alpha + \beta}{\beta}\right) + z^2}{\Sigma^2 (1 - z)} \\
&= \frac{\beta (z_+ - z) (z_- - z)}{\Sigma^2 (1 - z)}, \tag{2.29}
\end{aligned}$$

where we have defined  $\alpha = Q + L_z^2$  and  $\beta = a^2 (1 - E^2)$ . The quantities  $z_{\pm}$  are the two roots of the numerator in the second equation, satisfying

$$z_{\pm} = \frac{\alpha + \beta \pm \sqrt{(\alpha + \beta)^2 - 4Q\beta}}{2\beta}. \tag{2.30}$$

Note that  $z_+$  has a  $a^{-2}$  pole. This does not pose a problem, as the pole cancels out when  $z_+$  is incorporated into the equations of motion.

Next, we define  $z = z_- \cos^2 \chi$ . It is straightforward to compute  $d\chi/d\tau$  in terms of  $d\theta/d\tau$ ,

$$\frac{d\theta}{d\tau} = \sqrt{\frac{z_-}{1 - z}} \sin \chi \frac{d\chi}{d\tau}. \tag{2.31}$$

Substituting this expression directly into Eq. (2.29) and taking the square root (which we can again do without ambiguity), we obtain the following equation governing the evolution of  $\chi$ :

$$\frac{d\chi}{d\tau} = \frac{\sqrt{\beta (z_+ - z)}}{\Sigma}. \tag{2.32}$$

The pole in  $z_+$  is cancelled by the factor  $a^2$  in  $\beta$ . Equations (2.19), (2.20), (2.28), and (2.32) collectively represent the equations of motion around a Kerr black hole.

### The Geometric Significance of $\iota$

At this point, it is worthwhile to discuss the geometric significance of  $\iota$ . We already know the geometric interpretation of  $p$  and  $e$  as the semilatus rectum and eccentricity of an ellipse. Interestingly, the fact is that  $\iota$ , which is defined rather arbitrarily to satisfy  $Q = L_z^2 \tan^2 \iota$ , closely approximates the maximum value of  $|\frac{\pi}{2} - \theta|$  for orbits beyond about  $r \sim 3M$ . This should make some sense even without mathematical excavation; since  $Q$  can be regarded roughly as  $L_x^2 + L_y^2$ , the angle  $\iota$  corresponds approximately to the angle by which the normal vector of orbital plane is tipped relative to  $\vec{\mathbb{S}}$ .

The turning points of  $\theta$  occur where  $d\theta/d\tau = 0$ , so

$$\Theta(\theta_{\max}) = L_z^2 \tan^2 \iota - L_z^2 \cot^2 \theta_{\max} - a^2 (1 - E^2) \cos^2 \theta_{\max} = 0, \quad (2.33)$$

or

$$\tan^2 \iota - \cot^2 \theta_{\max} = \frac{a^2 (1 - E^2)}{L_z^2} \cos^2 \theta_{\max}. \quad (2.34)$$

The total energy of the particle is just slightly less than its rest energy for particles that are not too close to the black hole. In other words,  $E = 1 - E_{\text{bind}}$ , where  $E_{\text{bind}}$  is a small positive number on the order of 0.05 corresponding to the binding energy.<sup>6</sup> We can therefore drop terms like  $E_{\text{bind}}^2$  and write Eq. (2.34) as

$$\tan^2 \iota - \cot^2 \theta_{\max} \approx \frac{2a^2 E_{\text{bind}}}{L_z^2} \cos^2 \theta_{\max}. \quad (2.35)$$

In fact, we can take this approximation one step farther by noting that the right hand side of the Eq. (2.35) is nearly zero for the orbits considered in this thesis. As such, we can determine the relationship between  $\iota$  and  $\theta_{\max}$  to zeroth order in  $E_{\text{bind}}$ :

$$\tan^2 \iota \approx \cot^2 \theta_{\max}. \quad (2.36)$$

Since  $\cot \theta_{\max} = \tan(\frac{\pi}{2} - \theta_{\max})$ ,

$$\tan^2 \iota = \tan^2 \left( \frac{\pi}{2} - \theta_{\max} \right), \quad (2.37)$$

which immediately implies that  $\iota = \left| \frac{\pi}{2} - \theta_{\max} \right|$ . If we include the first order correction from  $E_{\text{bind}}$ , we find that the true  $\theta_{\max}$  corresponds to a particular  $\iota$  plus a small correction  $\delta\iota$ , which satisfies

$$\iota + \delta\iota = \left| \frac{\pi}{2} - \theta_{\max} \right|, \quad (2.38)$$

given to leading order in  $E_{\text{bind}}$  by

$$\delta\iota = \frac{\tan \iota}{2 + L_z^2 \sec^4 \iota / a^2 E_{\text{bind}}}. \quad (2.39)$$

For the orbits we study here,  $L_z^2 \sec^4 \iota / a^2 E_{\text{bind}} \gg 2$ , so

$$\delta\iota \approx \frac{a^2 E_{\text{bind}} \sin \iota \cos^3 \iota}{L_z^2}. \quad (2.40)$$

---

<sup>6</sup> $E_{\text{bind}}$  can become larger for extremely close orbits around rapidly rotating black holes. This is not an issue for orbits that lie outside about  $r \sim 3M$ , beyond which the asphericities of the Kerr metric are relatively insignificant.

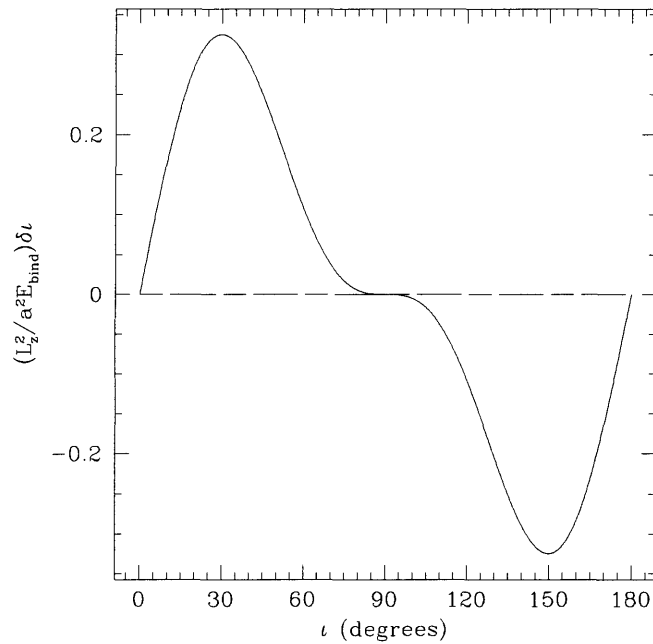


Figure 2-2: The discrepancy  $\delta l$  (in normalized units) between  $l$  and  $|\frac{\pi}{2} - \theta_{\max}|$ . The discrepancy is greatest near  $l = \pi/6$  and  $l = 5\pi/6$ .  $\delta l$  is never very large, so  $l$  is essentially equal to  $|\frac{\pi}{2} - \theta_{\max}|$ .

The maximum value of  $|\delta l|$  for our typical orbits around a maximally spinning ( $a = 1$ ) black hole is about  $3 \times 10^{-3}$  and occurs near  $l = \pi/6$  and  $l = 5\pi/6$  (see Fig. 2-2).

## 2.4 Momentum Equations

At various points in the code, we will find it handy to be able to calculate the four components of  $p_\mu$  of the particle. It is relatively easy to calculate the momentum components, since the definition of four-momentum requires that

$$\frac{p_\mu}{m} = g_{\mu\nu} \frac{dx^\nu}{d\tau}. \quad (2.41)$$

The  $t$  and  $\phi$  momenta are simple, since their values are fixed by definition;

$$p_t/m = -E \quad (2.42)$$

$$p_\phi/m = L_z. \quad (2.43)$$

The  $r$  and  $\theta$  momenta are slightly more complicated, but still straightforward to derive. Since the only non-zero component of  $g_{r\nu}$  is  $g_{rr}$ , the radial momentum  $p_r$  is given by

$$\begin{aligned} \frac{p_r}{m} &= g_{rr} \frac{dr}{d\tau} \\ &= \frac{\Sigma}{\Delta} \left( \frac{r^2 e \sin \psi}{p} \frac{d\psi}{d\tau} \right) \\ &= \frac{r e \sin \psi}{\Delta} \sqrt{\frac{(1-E^2)(r-r_0)(r-r_1)}{1-e^2}}. \end{aligned} \quad (2.44)$$

The  $\sin \psi$  in the numerator ensures that  $p_r$  has the correct sign at all times.

The only non-zero component of  $g_{\theta\nu}$  is  $g_{\theta\theta}$ , so the calculation of the polar momentum  $p_\theta$  proceeds in the same way as it did for  $p_r$ ,

$$\frac{p_\theta}{m} = g_{\theta\theta} \frac{d\theta}{d\tau} = \sqrt{\frac{\beta(z_+ - z)z_-}{1-z}} \sin \chi. \quad (2.45)$$

As with the radial momentum, the  $\sin \chi$  ensures that  $p_\theta$  has the right sign.<sup>7</sup>

## 2.5 Mapping between Constants

### 2.5.1 $(E, L_z, Q) \rightarrow (p, e, \iota)$

Our spin equations allow us to compute time derivatives of  $E$ ,  $L_z$ , and  $Q$ . We do not know *a priori* how spin couples to  $p$ ,  $e$ , and the inclination  $\iota$ . Accordingly, we would like to have our simulation continuously calculate  $p$ ,  $e$ , and  $\iota$  from  $E$ ,  $L_z$ , and  $Q$ . In other words,  $p$ ,  $e$ , and  $\iota$  are not stored as variables, but are rather functions of the correctly evolving  $E$ ,  $L_z$ , and  $Q$ .

We need an algorithm to effect this mapping. In fact, we have already worked out the difficult part; by factoring the radial equation, which is a quartic polynomial in  $r$  with coefficients that depend on  $E$ ,  $L_z$ , and  $Q$ , we find that the two radial turning points  $r_3$  and  $r_2$  correspond to  $p/(1-e)$  and  $p/(1+e)$ , respectively. Since  $r_3$  and  $r_2$  are computed entirely from  $E$ ,  $L_z$ , and  $Q$ , we can isolate  $p$

---

<sup>7</sup>The structure of the coordinate system we use is such that increasing the  $z$  coordinate corresponds to *decreasing*  $\theta$ . The same is true in normal spherical coordinates. This insight is crucial to understanding the relative phase of  $p_\theta$  and  $\theta$ , which should be exactly opposite the relative phase of  $p_r$  and  $r$ .

and  $e$  (and  $\iota$ , for which we do not need to invoke the root finder);

$$p = \frac{2r_3r_2}{r_3 + r_2} \quad (2.46)$$

$$e = \frac{r_3 - r_2}{r_3 + r_2} \quad (2.47)$$

$$\iota = \arctan\left(\sqrt{Q/L_z^2}\right). \quad (2.48)$$

Numerical factorization of  $R(r)$  is perhaps the easiest way to go. Tools for numerically factoring polynomials are widely available (see, e.g., the function `zroots` in Ref. [18]).

### The Analytic Method

If speed is a consideration, one can do as we have done and calculate the roots of the quartic radial equation analytically instead of numerically.<sup>8</sup> With  $c_3$ ,  $c_2$ ,  $c_1$ , and  $c_0$  defined as in Eq. (2.26), the analytical roots  $\tilde{r}_3$ ,  $\tilde{r}_2$ ,  $\tilde{r}_1$ , and  $\tilde{r}_0$  of the radial equation  $R(r)$  are given by

$$\tilde{r}_3 = -\frac{c_3}{4} - \frac{1}{2}\sqrt{\Omega_0} - \frac{1}{2}\sqrt{\Omega_1 - \Omega_2} \quad (2.49)$$

$$\tilde{r}_2 = -\frac{c_3}{4} - \frac{1}{2}\sqrt{\Omega_0} + \frac{1}{2}\sqrt{\Omega_1 - \Omega_2} \quad (2.50)$$

$$\tilde{r}_1 = -\frac{c_3}{4} + \frac{1}{2}\sqrt{\Omega_0} - \frac{1}{2}\sqrt{\Omega_1 + \Omega_2} \quad (2.51)$$

$$\tilde{r}_0 = -\frac{c_3}{4} + \frac{1}{2}\sqrt{\Omega_0} + \frac{1}{2}\sqrt{\Omega_1 + \Omega_2}, \quad (2.52)$$

with

$$\begin{aligned} \Omega_0 &= \Lambda_1 - \frac{2c_2}{3} + \frac{c_3^2}{4} \\ \Omega_1 &= -\Lambda_1 - \frac{4c_2}{3} + \frac{c_3^2}{2} \\ \Omega_2 &= \frac{-8c_1 + 4c_2c_3 - c_3^3}{4\sqrt{\Omega_0}} \\ \Lambda_1 &= \frac{12c_0 + c_2^2 - 3c_1c_3}{3\Lambda_2} + \frac{\Lambda_2}{3} \\ \Lambda_2 &= \left[ \Lambda_3 + \sqrt{\Lambda_3^2 - (12c_0 + c_2^2 - 3c_1c_3)^3} \right]^{1/3} \\ \Lambda_3 &= \frac{27c_1^2 - 72c_0c_2 + 2c_2^3 - 9c_1c_2c_3 + 27c_0c_3^2}{2}. \end{aligned}$$

The roots  $\tilde{r}_3$ ,  $\tilde{r}_2$ ,  $\tilde{r}_1$ , and  $\tilde{r}_0$  are not necessarily ordered as we need them to be, which is why we chose to call them  $\tilde{r}_i$  (with  $i = 0, 1, 2, 3$ ) instead of  $r_i$ . We simply need to equate the largest of the

<sup>8</sup>The performance gains of using an analytic approach are tremendous when the particle is subject to forces. Because  $E$ ,  $L_z$ , and  $Q$  change with time, the root finder must be called at each time step to compute the new  $p$ ,  $e$ , and  $\iota$ . Performing an iterative, numerical algorithm that many times will surely slow down the execution of the code. If one is considering only unperturbed geodesic trajectories, however,  $p$ ,  $e$ , and  $\iota$  are constant, so the root finder only needs to be run once at the beginning of the program.

$\tilde{r}_i$  with  $r_3$ , the second largest with  $r_2$ , and so on. From these  $r_i$  we can calculate  $p$  and  $e$  according to Eqs. (2.46) and (2.47). The inclination  $\iota$  is calculated as in Eq. (2.48).

### 2.5.2 $(p, e, \iota) \rightarrow (E, L_z, Q)$

We will also find it useful to have an inverse transformation for the initial time step. It is far easier to specify orbits in terms of geometric quantities like  $p$ ,  $e$ , and  $\iota$  than  $E$ ,  $L_z$ , and  $Q$ , so we would like to have a tool for converting the user-specified geometric constants into initial  $E$ ,  $L_z$ , and  $Q$ . Indeed, the key again lies in the radial equation,  $R(r)$ . By definition,  $R(r)$  must satisfy

$$\begin{aligned} R(r_3) &= 0 \\ R(r_2) &= 0, \end{aligned} \tag{2.53}$$

since  $r_3 = p/(1 - e)$  and  $r_2 = p/(1 + e)$  are the turning points.  $R(r)$  is a quartic function with coefficients determined by  $E$ ,  $L_z$ , and  $Q = L_z^2 \tan^2 \iota$ , and since  $\iota$  is specified along with  $p$  and  $e$ , we can replace all instances of  $Q$  in  $R(r)$  with  $L_z^2 \tan^2 \iota$ , leaving only  $E$  and  $L_z$  as unknowns in  $R(r) = 0$ . We solve for these two quantities with the Newton-Raphson method (see, e.g., the function `mnewt` in Ref. [18]), which requires us to specify initial guesses for the energy and angular momentum. The algorithm depends sensitively on the initial guesses, but since  $E$  and  $L_z$  do not vary by much over our allowed range, we can get away with using the energy and angular momentum of circular orbits ( $e = 0$ ). Thus,

$$E^{\text{guess}} = E^{\text{circ}}(r = p) \tag{2.54}$$

$$L_z^{\text{guess}} = L_z^{\text{circ}}(r = p). \tag{2.55}$$

An alternate approach which is quite common is to set  $r = p/(1 - e^2)$ , which corresponds to the semi-major axis of the ellipse. Fortunately, there are simple analytic expressions for the energy and angular momentum of circular, equatorial orbits (see Ref. [19]). We can use these analytic expressions as initial guesses to the energy and angular momentum of generic inclined, eccentric orbits. In particular, we use the energy and angular momentum associated with *prograde* circular, equatorial orbits (defined by  $L_z > 0$ ),<sup>9</sup> so that the initial guesses are

$$E^{\text{pro}} = \frac{1 - 2w^2 + jw^3}{\sqrt{1 - 3w^2 + 2jw^3}} \tag{2.56}$$

$$L_z^{\text{pro}} = rw \frac{1 - 2jw^3 + j^2w^4}{\sqrt{1 - 3w^2 + 2jw^3}}, \tag{2.57}$$

---

<sup>9</sup>We use the prograde angular momentum because retrograde orbits do not always exist. In particular, close orbits around rapidly rotating black holes that cross into the ergosphere are not permitted to orbit in the retrograde direction. It is therefore wise to use prograde orbits as the basis of the initial guesses, since prograde orbits always exist.

where  $w = \sqrt{M/r}$  and  $j = a/M$  [20]. Naturally, the label “pro” reflects the fact that these quantities are defined for prograde orbits. These initial guesses work well, permitting the Newton-Raphson method to compute  $E$ ,  $L_z$ , and  $Q$  robustly and reliably from  $p$ ,  $e$ , and  $\iota$ .

The corresponding quantities for retrograde orbits,

$$E^{\text{ret}} = \frac{1 - 2w^2 - jw^3}{\sqrt{1 - 3w^2 - 2jw^3}} \quad (2.58)$$

$$L_z^{\text{ret}} = -rw \frac{1 + 2jw^3 + j^2w^4}{\sqrt{1 - 3w^2 - 2jw^3}}, \quad (2.59)$$

should also work well as initial guesses, except for orbits that lie within the ergosphere of the black hole. The best initial guesses may involve some linear combination of prograde and retrograde guesses with coefficients that may depend on the inclination angle  $\iota$ .

## 2.6 Finding the Least Stable Orbit

In general relativity, a particle cannot orbit within some minimum distance of the central black hole without falling in. To ensure that the orbits we specify are stable, it is necessary to have a function for computing the least stable orbit.

Mathematically, the least stable orbit occurs when  $r_1 = r_2$ ;  $r_1$ , the larger of the two “inner roots” of  $R(r)$  slides out to the periastron distance  $r_2 = p/(1 + e)$ , forming a minimum rather than a zero crossing (see Fig. 2-3). Accordingly, the least stable orbit is characterized by a constraint on  $\partial R(r)/\partial r$  as well as the two standard constraints on  $R(r)$  that all stable orbits must satisfy:

$$\begin{aligned} R(r_3) &= 0 \\ R(r_2) &= 0 \\ \left. \frac{\partial R(r)}{\partial r} \right|_{r=r_2} &= 0. \end{aligned} \quad (2.60)$$

The first two conditions allow us to determine  $E$ ,  $L_z$ , and  $Q = L_z^2 \tan^2 \iota$  from a given  $p$ ,  $e$ , and  $\iota$ , but the extra condition eliminates the need for us to specify  $p$ . As such, we need only specify  $e$  and  $\iota$  in order to infer the values of  $E$ ,  $L_z$ ,  $Q$ , and  $p$  associated with the least stable orbit. We label this least stable  $p$  suggestively as  $p_{\text{LSO}}$ ; the “LSO” stands for “least stable orbit.” If  $p$  is chosen to be less than  $p_{\text{LSO}}$ , the radial quasi-potential implies the non-sensical result that  $dr/d\tau$  is imaginary (see Fig. 2-4).

### Initial Guesses

As before, we must specify initial guesses for all quantities we wish to determine. The energy and angular momentum guesses are specified as before (specifically,  $E^{\text{guess}} = E^{\text{pro}}$  and  $L_z^{\text{guess}} = L_z^{\text{pro}}$ ).

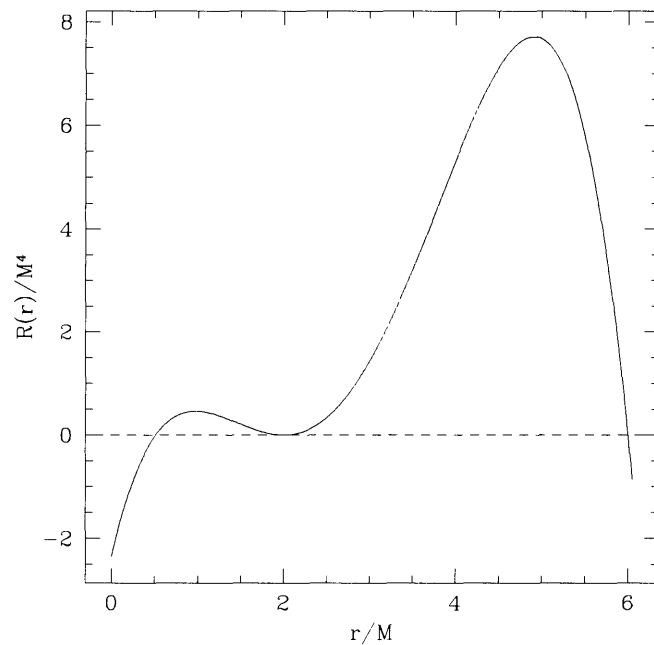


Figure 2-3:  $R(r)$  for a marginally stable orbit around a black hole with  $a = 0.95M$ . The orbit has  $p = 3M$  and  $e = 0.5$  as in Fig. 2-1, but  $\iota$  has been increased to  $40.751^\circ$ . Note that the larger of the two inner roots  $r_1$  has moved so far to the right that it now coincides with periastron,  $r_2$ , forming a minimum instead of a zero crossing. As this point,  $\partial R(r)/\partial r = 0$ . Figure adapted from Ref. [15].

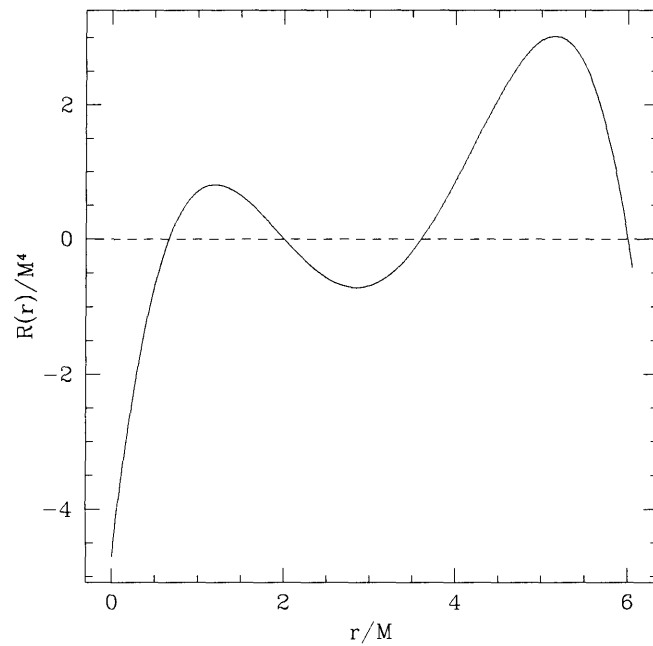


Figure 2-4:  $R(r)$  for an unstable orbit around a black hole with  $a = 0.95M$ . The orbit is still characterized by  $p = 3M$  and  $e = 0.5$ , but  $\iota$  is now  $55^\circ$ . Note that the physically inaccessible root  $r_1$  has moved past  $r_2$  and become accessible; the particle now orbits between  $r_1$  and  $r_3$ , and periastron no longer occurs at  $r = 2M$ . Figure adapted from Ref. [15].

The initial guess we use for  $p_{\text{LSO}}$  is

$$p_{\text{LSO}}^{\text{guess}} = (6 + 2e)M, \quad (2.61)$$

which corresponds to the innermost stable orbit around a Schwarzschild black hole. This guess generally works well, but there is some evidence that it fails for values of  $a$  very close to  $M$ . It might therefore be more appropriate to use as an initial guess the innermost stable *circular* orbit around a Kerr black hole [19],

$$p_{\text{LSO}}^{\text{guess}} = 3M + Z_2 - \sqrt{(3M - Z_1)(3M + Z_1 + 2Z_2)}, \quad (2.62)$$

with

$$Z_1 = M + \sqrt[3]{M^2 - a^2} \left( \sqrt[3]{M + a} + \sqrt[3]{M - a} \right) \quad (2.63)$$

$$Z_2 = \sqrt{3a^2 + Z_1^2}. \quad (2.64)$$

This guess appears to be slightly more robust than  $p_{\text{LSO}}^{\text{guess}} = (6 + 2e)M$ . There is, however, no guarantee that this guess will work well for highly eccentric or inclined orbits. All we have for now are the two analytically-known limits of  $p_{\text{LSO}}$  for  $a \rightarrow 0$  or  $e, \iota \rightarrow 0$ . Whichever limit we chose to use as our initial guess, we risk faulty results if the initial guess is too far from the actual  $p_{\text{LSO}}$ .

To generate a better initial guess, we propose the following *ansatz* for  $p_{\text{LSO}}$ :

$$p_{\text{LSO}}^{\text{guess}} = \left[ 3M + Z_2 - \sqrt{(3M - Z_1)(3M + Z_1 + 2Z_2)} \right] \left( \frac{6 + 2e}{6} \right). \quad (2.65)$$

If  $e = 0$ , the guess is the same as the analytically known limit in Eq. (2.61). Alternatively, if  $a = 0$ , the guess reduces to Eq. (2.62). To formulate an even more robust initial guess, it may be helpful to include some dependence on  $\iota$ . We do not consider this issue further since the simple initial guesses in Eqs. (2.61) and (2.62) work well enough for our purposes; the preceding discussion serves only as a guideline for other work with more stringent requirements.

## 2.7 Integration

A standard geodesic integrator is nothing more than a set of routines for evolving  $\psi$ ,  $\chi$ , and  $\phi$  in terms of the coordinate time  $t$  along with functions for converting between  $(p, e, \iota)$  and  $(E, L_z, Q)$ . Our code integrates the derivatives of  $\psi$ ,  $\chi$ , and  $\phi$  using the Bulirsch-Stoer method (see, e.g., Ref. [18]),

starting with the initial values

$$\psi(t = 0) = 0 \quad \chi(t = 0) = 0 \quad \phi(t = 0) = 0, \quad (2.66)$$

which implies that the particle starts out at periastron with maximum possible distance from the equatorial plane.

### 2.7.1 Incorporating Spin

The novelty of our code is that, in addition to evolving  $\psi$ ,  $\chi$ , and  $\phi$ , we also integrate derivatives of  $E$ ,  $L_z$ ,  $Q$  and components of the spin tensor  $S^{\mu\nu}$ , all of which we will calculate in Chapter 3. Extending our code to handle small body spin is simply a matter of letting these quantities vary according to the equations we derive instead of holding them fixed.

It is worthwhile to mention explicitly that the Papapetrou equations for spin allow us to determine the derivatives of  $E$ ,  $L_z$ , and  $Q$ , *but not*  $p$ ,  $e$ , or  $\iota$ .<sup>10</sup> The latter three quantities must be calculated continuously from  $E$ ,  $L_z$ , and  $Q$  using the analytic root finder and the definition  $Q = L_z^2 \tan^2 \iota$ . As such, it is perhaps most useful to think of  $p$ ,  $e$ , and  $\iota$  as convenient functions of  $E$ ,  $L_z$ , and  $Q$ .

---

<sup>10</sup>In actuality, with the analytic transformation from  $(E, L_z, Q)$  to  $(p, e, \iota)$ , it is possible in principle to calculate the derivatives of the geometric constants. Based on the complexity of the quartic solution, however, it is probably not practical except in the case of  $\iota$ , which has a particularly simple relationship to  $L_z$  and  $Q$ . Besides, the  $(E, L_z, Q) \rightarrow (p, e, \iota)$  transformation is unique, but not one-to-one—prograde and retrograde orbits with different  $(E, L_z, Q)$  can map to the same set  $(p, e, \iota)$ . It is therefore advantageous to use the  $(E, L_z, Q) \rightarrow (p, e, \iota)$  transformation exclusively.

## Chapter 3

# Spin and Orbital Evolution

In this chapter, we explore the issue of spin in greater depth than we did in Chapter 1. We will provide the specific and detailed equations governing the evolution of the orbital constants that is induced by the existence of spin on the small body. Since the spin itself varies with time due to precession, we will also work out similar equations for the evolution of the spin tensor components. We will also consider one special case in which the evolution equations are especially simple.

### 3.1 Mathematical Basis of Spin

At a physical level, we are used to thinking of spin as a vector quantity. Indeed, the spin of an orbiting particle can be written as a vector  $S^\mu$  (or as a one-form  $S_\mu = g_{\mu\nu}S^\nu$ , which is what we do for reasons that will soon be clear). In a generic sense, spin has a magnitude and direction, but nothing else.

At this point, one may justifiably wonder why, in the previous chapters, we wrote the small body spin as tensor instead of a vector. The reason is quite simple and has to do with aesthetics; the Papapetrou equations are much simpler when expressed in terms of  $S^{\mu\nu}$ . Using  $S^{\mu\nu}$  in place of  $S_\mu$  is no cause for alarm, but we do need to describe how one constructs  $S^{\mu\nu}$  from  $S_\mu$ . The definition turns out to be relatively simple;

$$S^{\mu\nu} = \epsilon^{\mu\nu\sigma\lambda} S_\lambda p_\sigma, \quad (3.1)$$

where  $\epsilon^{\mu\nu\sigma\lambda}$  is the totally antisymmetric Levi-Civita symbol. This four-index object is the obvious generalization of the three-index symbol, with  $\epsilon^{tr\theta\phi} = 1$ . Note that the antisymmetry of  $\epsilon^{\mu\nu\sigma\lambda}$

carries over to  $S^{\mu\nu}$ . According to this definition,

$$\begin{aligned}
S^{\mu\nu} &= \begin{pmatrix} 0 & S^{tr} & S^{t\theta} & S^{t\phi} \\ -S^{tr} & 0 & S^{r\theta} & S^{r\phi} \\ -S^{t\theta} & -S^{r\theta} & 0 & S^{\theta\phi} \\ -S^{t\phi} & -S^{r\phi} & -S^{\theta\phi} & 0 \end{pmatrix} \\
&= \begin{pmatrix} 0 & S_\phi p_\theta - S_\theta p_\phi & S_r p_\phi - S_\phi p_r & S_\theta p_r - S_r p_\theta \\ \circ & 0 & S_\phi p_t - S_t p_\phi & S_t p_\theta - S_\theta p_t \\ \circ & \circ & 0 & S_r p_t - S_t p_r \\ \circ & \circ & \circ & 0 \end{pmatrix}, \tag{3.2}
\end{aligned}$$

where each  $\circ$  entry is the negative of its partner in the upper-triangular part of  $S^{\mu\nu}$ . The quantities  $p_r$  and  $p_\theta$  can be easily calculated from Eqs. (2.44) and (2.45).

## 3.2 Evolution of Orbital Constants

### 3.2.1 Evolution of the Energy and Angular Momentum

According to the Papapetrou equations,

$$\frac{Dp_\mu}{D\tau} = f_\mu = -\frac{1}{2}R_{\mu\nu\alpha\beta}v^\nu S^{\alpha\beta}. \tag{3.3}$$

Since  $E = -p_t$  and  $L_z = p_\phi$ , we can essentially read the evolution equations for these two quantities directly from Eq. (3.3):

$$\frac{dE}{d\tau} = \frac{DE}{D\tau} = \frac{1}{2}R_{t\nu\alpha\beta}v^\nu S^{\alpha\beta} = -\frac{1}{2}T^\mu R_{\mu\nu\alpha\beta}v^\nu S^{\alpha\beta} \tag{3.4}$$

$$\frac{dL_z}{d\tau} = \frac{DL_z}{D\tau} = -\frac{1}{2}R_{\phi\nu\alpha\beta}v^\nu S^{\alpha\beta} = -\frac{1}{2}\Phi^\mu R_{\mu\nu\alpha\beta}v^\nu S^{\alpha\beta}. \tag{3.5}$$

Essentially, all we have done here is to identify the  $\mu$  component of the force with the  $\mu$  component of the change in momentum.<sup>1</sup>

---

<sup>1</sup>The  $r$  and  $\theta$  components of the force are slightly more complicated. The formal expansion of the covariant derivative yields  $\frac{dp_\mu}{d\tau} = -\frac{1}{2}R_{\mu\nu\alpha\beta}v^\nu S^{\alpha\beta} - \frac{1}{2}p^\sigma v^\nu \partial_\mu g_{\nu\sigma}$ , which reduces to Eqs. (3.4) and (3.5) when  $\mu = t$  or  $\mu = \phi$ , since  $g_{\mu\nu}$  is independent of both. The second term is non-zero if  $\mu = r$  or  $\mu = \theta$ .

### 3.2.2 Evolution of the Carter Constant

There are two ways to construct the derivative  $dQ/d\tau$ . With the first approach, we can use Eq. (1.33) and simply substitute the force equation from Eq. (1.40), which yields

$$\dot{Q} = -p_\lambda [K^{\mu\lambda} - (\Phi^\mu - aT^\mu)(\Phi^\lambda - aT^\lambda)] R_{\mu\nu\alpha\beta} v^\nu S^{\alpha\beta}. \quad (3.6)$$

This is perhaps the most straightforward way to compute  $dQ/d\tau$ .

There is, however, an alternative method mentioned by Tanaka *et al.* [21] which uses the anti-symmetric Killing-Yano tensor

$$f_{\mu\nu} = 2a \cos\theta e_{[\mu}^1 e_{\nu]}^0 + 2re_{[\mu}^2 e_{\nu]}^3, \quad (3.7)$$

where

$$e_\mu^0 = \left( \sqrt{\frac{\Delta}{\Sigma}}, 0, 0, -a \sin^2\theta \sqrt{\frac{\Delta}{\Sigma}} \right) \quad (3.8)$$

$$e_\mu^1 = \left( 0, \sqrt{\frac{\Sigma}{\Delta}}, 0, 0 \right) \quad (3.9)$$

$$e_\mu^2 = \left( 0, 0, \sqrt{\Sigma}, 0 \right) \quad (3.10)$$

$$e_\mu^3 = \left( -\frac{a}{\sqrt{\Sigma}} \sin\theta, 0, 0, \frac{r^2 + a^2}{\Sigma} \sin\theta \right) \quad (3.11)$$

define the tetrad frame. The tensor  $f_{\mu\nu}$  is related to  $K_{\mu\nu}$  by

$$K_{\mu\nu} = f_{\mu\sigma} f_\nu^\sigma. \quad (3.12)$$

It is also helpful to define

$$f_{\mu\nu\sigma} = \nabla_\sigma f_{\mu\nu} = 6 \left( \frac{a \sin\theta}{\sqrt{\Sigma}} e_{[\mu}^0 e_\nu^1 e_{\sigma]}^2 + \sqrt{\frac{\Delta}{\Sigma}} e_{[\mu}^1 e_\nu^2 e_{\sigma]}^3 \right), \quad (3.13)$$

in which case

$$\frac{dQ}{d\tau} = 2 \frac{d}{d\tau} [p^\mu (f_\sigma^\nu f_{\mu\rho\nu} - f_\mu^\nu f_{\rho\sigma\nu}) S^{\rho\sigma}]. \quad (3.14)$$

In effecting this derivative, we assume  $E$  and  $L_z$  are constant—this after all is expected of any parameter that varies mildly. We adopt the approach of Tanaka *et al.* in this thesis, but the first method should produce equivalent results.

Daunting as Eqs. (3.4), (3.5), and (3.14) may look, they are relatively straightforward to evaluate using the Kerr metric  $g_{\mu\nu}$ , since  $R_{\lambda\nu\alpha\beta}$  can be expressed entirely in terms of  $g_{\mu\nu}$  and its derivatives.

The expression is universally-known, but largely unrelated to the present discussion. As such, we refer the reader to Refs. [10] and [11] for the necessary detail.

### Equatorial Orbits

One troubling aspect of this evolutionary scheme must be mentioned, however. For equatorial orbits,  $Q = 0$ . This is numerically worrisome because  $Q$  cannot be less than zero (it is defined as  $Q = L_z^2 \tan^2 \iota$ ), and so the equatorial  $Q$  is riding exactly on the boundary of what is physically allowed. But since our equations of motion are valid only to linear order in  $S$ , it is entirely possible that  $dQ/d\tau$  is slightly negative in the equatorial plane. In practice, this happens quite a lot;  $Q$  falls below zero and the code crashes. If one wishes to explore equatorial orbits, the best course of action is to explicitly set  $dQ/d\tau = 0$ . Our simulations all occur at non-zero inclination, so we mention this cautionary fact only to highlight a circumventable weakness in the whole scheme. No such weakness affects  $E$  or  $L_z$ .

### 3.2.3 Evolution of the Spin Tensor

The derivation of the equations governing the evolution of  $S^{\mu\nu}$  proceeds as expected. Starting off with the spin part of the Papapetrou equations, we have that

$$\frac{DS^{\mu\nu}}{D\tau} = \frac{dS^{\mu\nu}}{d\tau} + v^\sigma \Gamma_{\sigma\lambda}^\mu S^{\lambda\nu} + v^\sigma \Gamma_{\sigma\lambda}^\nu S^{\mu\lambda} = 0. \quad (3.15)$$

It is easy to solve this equation for  $dS^{\mu\nu}/d\tau$ , since

$$\frac{dS^{\mu\nu}}{d\tau} = v^\sigma (\Gamma_{\sigma\lambda}^\nu S^{\lambda\mu} - \Gamma_{\sigma\lambda}^\mu S^{\lambda\nu}). \quad (3.16)$$

One can leave the equation in this state, or write it entirely in terms of  $g_{\mu\nu}$ . To do so, we must identify  $\Gamma_{\sigma\lambda}^\nu = \frac{1}{2}g^{\nu\rho} (\partial_\sigma g_{\rho\lambda} + \partial_\lambda g_{\rho\sigma} - \partial_\rho g_{\lambda\sigma})$ , we can simplify the evolution equation to

$$\frac{dS^{\mu\nu}}{d\tau} = \frac{1}{2}v^\sigma (\partial_\sigma g_{\rho\lambda} + \partial_\lambda g_{\rho\sigma} - \partial_\rho g_{\lambda\sigma}) (g^{\nu\rho} S^{\lambda\mu} - g^{\mu\rho} S^{\lambda\nu}). \quad (3.17)$$

It is probably the case that this expression can be simplified even further. However, we refrain from doing so here since Eq. (3.17) can be implemented numerically with relative ease.

### 3.3 Supplementary Equations

#### 3.3.1 Center of Mass Constraint

The Papapetrou equations are typically supplemented with the center of mass constraint,

$$p_\mu S^{\mu\nu} = 0. \quad (3.18)$$

Writing out the four equations stored in Eq. (3.18), we have

$$\begin{aligned} p_t S^{tt} + p_r S^{rt} + p_\theta S^{\theta t} + p_\phi S^{\phi t} &= 0 \\ p_t S^{tr} + p_r S^{rr} + p_\theta S^{\theta r} + p_\phi S^{\phi r} &= 0 \\ p_t S^{t\theta} + p_r S^{r\theta} + p_\theta S^{\theta\theta} + p_\phi S^{\phi\theta} &= 0 \\ p_t S^{t\phi} + p_r S^{r\phi} + p_\theta S^{\theta\phi} + p_\phi S^{\phi\phi} &= 0. \end{aligned}$$

By exploiting the antisymmetry of  $S^{\mu\nu}$ , we can rewrite these equations entirely in terms of the upper triangular elements of  $S^{\mu\nu}$ :

$$-p_r S^{tr} - p_\theta S^{t\theta} - p_\phi S^{t\phi} = 0 \quad (3.19)$$

$$p_t S^{tr} - p_\theta S^{r\theta} - p_\phi S^{r\phi} = 0 \quad (3.20)$$

$$p_t S^{t\theta} + p_r S^{r\theta} - p_\phi S^{\theta\phi} = 0 \quad (3.21)$$

$$p_t S^{t\phi} + p_r S^{r\phi} + p_\theta S^{\theta\phi} = 0. \quad (3.22)$$

Only three of these four equations are independent. After noting that  $p_t = -E$  and  $p_\phi = L_z$ , we can eliminate any three of the spin tensor components. We eliminate  $S^{tr}$ ,  $S^{t\theta}$ , and  $S^{t\phi}$  by identifying:

$$S^{tr} = \frac{-L_z S^{r\phi} - p_\theta S^{r\theta}}{E} \quad (3.23)$$

$$S^{t\theta} = \frac{p_r S^{r\theta} - L_z S^{\theta\phi}}{E} \quad (3.24)$$

$$S^{t\phi} = \frac{p_r S^{r\phi} + p_\theta S^{\theta\phi}}{E}. \quad (3.25)$$

We have already worked out the method of calculating  $p_r$  and  $p_\theta$  in Section 2.4, so one can calculate the three  $S^{t\mu}$  from the other three components at any time with relative ease.

However, there is a perfectly good reason to *not* apply the center of mass constraint, which is typically enforced in order to deal with the discrepancy between  $u^\mu$  and  $v^\mu$  that is present when the Papapetrou equations are written out to second order in  $S$ . In particular,  $p_\mu S^{\mu\nu} = 0$  allows one to compute  $p^\mu$  from  $v^\mu$ . In our first-order analysis, however,  $p^\mu$  and  $v^\mu$  are parallel, and the constraint

is unnecessary.<sup>2</sup> This raises a question about the precise meaning of the center of mass, which we will consider in Chapter 4.

### 3.3.2 Spin Magnitude

Finally, we must derive an expression for  $S^2$  which we can use to monitor the magnitude of the spin. The calculation can be set up with a minimum of difficulty:

$$S^2 = \frac{1}{2} S_{\mu\nu} S^{\mu\nu} = \frac{1}{2} g_{\mu\alpha} g_{\nu\beta} S^{\alpha\beta} S^{\mu\nu}. \quad (3.26)$$

With the Kerr metric  $g_{\mu\nu}$  in hand, it can be shown that

$$\begin{aligned} S^2 = & \gamma \sin^2 \theta \left[ \left( S^{\theta\phi} + \frac{2aMr}{\gamma} S^{t\theta} \right)^2 + \frac{1}{\Delta} \left( S^{r\phi} + \frac{2aMr}{\gamma} S^{tr} \right)^2 \right] + \frac{(S^{r\theta})^2 \Sigma^2}{\Delta} \\ & + \left[ (S^{t\theta})^2 + \frac{(S^{tr})^2}{\Delta} + \frac{(S^{t\phi})^2 \gamma \sin^2 \theta}{\Sigma^2} \right] \left( 2Mr - \frac{4a^2 M^2 r^2 \sin^2 \theta}{\gamma} - \Sigma \right), \end{aligned} \quad (3.27)$$

where

$$\begin{aligned} \Sigma &= r^2 + a^2 \cos^2 \theta \\ \Delta &= r^2 - 2Mr + a^2 \\ \gamma &= (r^2 + a^2)^2 - a^2 \Delta \sin^2 \theta. \end{aligned}$$

The magnitude of the spin (i.e., the square root of  $S^2$ ) has units of  $mM$ . Once we allow the spin to couple to the spacetime curvature, we find that  $S^2$  is not strictly constant. If we performed the full Papapetrou integration out to second order,  $S^2$  *would* be conserved.

## 3.4 Spin-Parallel Particle in the Equatorial Plane

In this section we will derive the equations of motion for the special case of a particle with spin vector pointed in the  $\pm \vec{e}_\theta$  direction orbiting in the equatorial plane. For such a particle, the only non-zero component of  $S_\mu$  is  $S_\theta$ , which allows us to considerably simplify the evolution equations. Furthermore, an equatorial spin-parallel particle provides an extremely pure test of spin interactions, since the particle can be “spin up” ( $S_\theta < 0$ ) or “spin down” ( $S_\theta > 0$ ). This configuration also allows a direct comparison to be made to electromagnetic interactions.

---

<sup>2</sup>Again,  $p^\mu$  and  $v^\mu$  *must* be parallel in our scheme, and so it is *incorrect* to apply the constraint since converting between  $p^\mu$  and  $v^\mu$  is trivial. It should only be applied when  $p^\mu$  and  $v^\mu$  are not parallel.

### 3.4.1 Orbital Evolution

For such an equatorial spin-parallel, we can write the spin tensor as

$$S^{\mu\nu} = \begin{pmatrix} 0 & -L_z S_\theta & 0 & S_\theta p_r \\ L_z S_\theta & 0 & 0 & E S_\theta \\ 0 & 0 & 0 & 0 \\ S_\theta p_r & -E S_\theta & 0 & 0 \end{pmatrix}. \quad (3.28)$$

Here we note that

$$S^{tr} = -\frac{L_z S^{r\phi}}{E} \quad (3.29)$$

$$S^{t\phi} = \frac{p_r S^{r\phi}}{E}, \quad (3.30)$$

With these relations in hand, the expression for  $S^2$  can be written entirely in terms of a single spin component,  $S^{r\phi}$ . We can of course use any one of the non-zero components in place of  $S^{r\phi}$ ; our choice is arbitrary. Making the appropriate substitutions yields

$$S^2 = \left[ \frac{\gamma}{\Delta} \left( 1 - \frac{2aM L_z r}{E\gamma} \right)^2 + \frac{1}{E^2} \left( \frac{L_z^2}{\Delta} + \frac{\gamma p_r^2}{r^4} \right) \left( 2Mr - \frac{4a^2 M^2 r^2}{\gamma} - r^2 \right) \right] (S^{r\phi})^2, \quad (3.31)$$

with  $\gamma$  now equal to  $(r^2 + a^2)^2 - a^2 \Delta$ .

After considerable simplification of Eqs. (3.4), (3.5), and (3.17), we can write

$$\frac{dE}{d\tau} = -\frac{3(aE - L_z)M\Delta p_r S^{r\phi}}{E r^5} \quad (3.32)$$

$$\frac{dL_z}{d\tau} = -\frac{3a(aE - L_z)M\Delta p_r S^{r\phi}}{E r^5} = a \frac{dE}{d\tau} \quad (3.33)$$

$$\frac{dS^{r\phi}}{d\tau} = -S^{r\phi} \frac{\Delta p_r}{r^3}. \quad (3.34)$$

The derivatives of the other non-zero components can be inferred from  $dS^{r\phi}/d\tau$  if necessary. Note also that for this special case,  $Q$  is always zero, hence we can say

$$\frac{dQ}{d\tau} = 0 \quad (3.35)$$

without actually carrying out the lengthy calculation in Eq. (3.14).

### 3.4.2 Analytic Integration

Because of the simple form of the evolution equations in the equatorial case, we can integrate the orbital and spin evolution equations analytically. First, however, we must use Eq. (2.44) and write

$$p_r = \frac{\Sigma}{\Delta} \frac{dr}{d\tau} = \frac{r^2}{\Delta} \frac{dr}{d\tau}. \quad (3.36)$$

Replacing all instances of  $p_r$  in the evolution equations with this expression, we find

$$\frac{dE}{d\tau} = -\frac{3(aE - L_z)MS^{r\phi}}{Er^3} \frac{dr}{d\tau} \quad (3.37)$$

$$\frac{dL_z}{d\tau} = a \frac{dE}{d\tau} \quad (3.38)$$

$$\frac{dS^{r\phi}}{d\tau} = -\frac{S^{r\phi}}{r} \frac{dr}{d\tau}. \quad (3.39)$$

Equations (3.38) and (3.39) immediately imply that

$$L_z = aE + A \quad (3.40)$$

$$S^{r\phi} = \frac{B}{r}, \quad (3.41)$$

where  $A$  and  $B$  are integration constants. We then rewrite Eq. (3.37) as

$$\frac{dE}{d\tau} = \frac{3ABM}{Er^4} \frac{dr}{d\tau}, \quad (3.42)$$

or multiplying through by  $E$ ,

$$E \frac{dE}{d\tau} = \frac{3ABM}{r^4} \frac{dr}{d\tau}. \quad (3.43)$$

This last expression can be integrated easily, yielding

$$E = \sqrt{C^2 - \frac{2ABM}{r^3}}, \quad (3.44)$$

where  $C^2$  is a third integration constant. Because  $B = 0$  for a spinless particle, we can interpret  $C$  as the energy of the particle minus the contribution of spin. At large radii, Eq. (3.44) implies

$$E \approx C - \frac{ABM}{Cr^3}. \quad (3.45)$$

The second term in this expression, which corresponds to the spin interaction energy, behaves very much like coupling of a magnetic dipole to an external electromagnetic field. In particular, both contain the same  $B/r^3$ , where  $B$  is a measure of the mass dipole or magnetic dipole. Equation (3.45)

implies that a spin down particle ( $B > 0$ ) is more tightly bound than a spin up particle ( $B < 0$ ).

With this information, we can compute  $S^2$  from Eq. (3.31):

$$S^2 = \frac{B^2}{C^2 - 2ABM/r^3}, \quad (3.46)$$

which implies that the total spin *increases* as the particle moves closer to the black hole. This is an obvious problem;  $S^2$  is supposed to be constant along a geodesic. But in fact the orbit is not a geodesic—the particle sloshes among adjacent geodesics due to the perturbative force—and so  $S^2$  is not fixed. If, on the other hand, the spin is decoupled from the orbit so that  $E$ ,  $L_z$ , and  $Q$  do not evolve, one would certainly expect  $S^2$  to remain fixed at its initial value. This issue will be described in greater detail in Chapter 4, but for now we note that the deviation from constancy is extremely small for orbits with large radii or small spin. Supposing that  $B$  is small, we can expand Eq. (3.46) to

$$S^2 \approx \frac{B^2}{C^2} + \frac{2AB^3M}{C^4r^3}. \quad (3.47)$$

The first term here is a true constant. The second term is radius-dependent but is suppressed by an additional factor of  $S$  over the first term. As one approaches  $S = 0$ , one quickly recovers unperturbed geodesic motion along which  $S^2$  should indeed be conserved. The second term in Eq. 3.47 drops to zero faster than the first term, and so  $S^2$  is very nearly conserved as one approaches the geodesic limit.



## Chapter 4

# Results and Discussion

### 4.1 A Prefatory Word on Spin

The spin on the small body is supposed to be a perturbative element, and therefore, we can reliably simulate orbits only when  $S$  is small. However, we use spins ranging from  $S = 10^{-3} mM$  all the way to  $S = 0.5 mM$ . This abuse of perturbation theory is not necessarily a problem, provided we bear in mind its limitations. Indeed, since our ultimate goal is to obtain an understanding of the various timescales that characterize the effect of spin, we can take  $S$  to be relatively close to 1 without much worry. All we are doing, in essence, is turning up the size of the perturbation to study it in detail, all while remembering that “real” orbits with smaller  $S$  demonstrate the same behavior but to a much lesser degree. If our goal was instead to compute orbits with high phase accuracy, the story would be very different, and making  $S$  too large would cause significant problems.

### 4.2 Code Validation

In order to verify that the code is working properly, we administered a series of tests to ensure that it produces sensible results in certain known limits. First, we analyzed the convergence properties of the algorithm in the limit  $S \rightarrow 0$ . In that limit, the spin-enhanced orbits should increasingly resemble the geodesic trajectories to which they correspond. Second, we examined the behavior of  $S^2$  in a “full” simulation (i.e., one in which all six components of the spin tensor are allowed to evolve independently) and compared it to the case in which three of the components are fixed by the center of mass constraint. Finally, we verified that the code behaves as expected when the effects of spin are decoupled from the particle’s trajectory.

### 4.2.1 Convergence

The first test we administered examined the convergence properties of the simulation. Specifically, we turned down the spin parameter  $S$  to check that the orbits gradually converged to the unperturbed geodesic trajectory. In all cases, the convergence was fantastic; even with  $S = 10^{-2} mM$ , which is a relatively large spin, the spin-enhanced orbit was virtually indistinguishable from the geodesic (see, e.g., Fig. 4-1). More than providing just a diagnostic check of our code, the rapid convergence properties of spin-enhanced orbits imply that the orbits of real spinning test particles are simply not all that different from pure geodesic trajectories. If ever there was a system amenable to study through perturbation theory, this is it.

### 4.2.2 Constrained Orbits

In the second test, we examine the behavior of  $S^2$  along orbits that are constrained by the center of mass condition ( $p_\mu S^{\mu\nu} = 0$ ) and compare it to the case in which all six spin tensor components are allowed to evolve independently. Even though  $S^2$  is not strictly conserved along the orbit, we expect that it will not deviate too far from a constant value.

The results of this comparative analysis were somewhat surprising. Even though the center of mass constraint does not strictly apply to orbits that are effectively jumping between geodesics, the value of  $p_\mu S^{\mu\nu}$  should not deviate too far from zero, and so we expected that enforcing the constraint would have a relatively mild effect on the orbit. Such is not the case by a long shot. Imposing the center of mass constraint effectively opposes the tendency of the particle to move around within the space of permissible geodesics, thereby introducing a fictitious but very significant pseudo-force on the particle. The severity of the problem can be seen by comparing the time dependence of  $S^2$  for the case in which the constraint is enforced to that in which it is not (see Fig. 4-2). Enforcing the constraint leads to much larger variations in  $S^2$  than are acceptable—the magnitude of the variation is forty times greater than the initial value of  $S^2$ ! The variations in  $S^2$  observed for the unconstrained orbits are *much* smaller. As such, we are forced to concede that it is inappropriate to enforce  $p_\mu S^{\mu\nu} = 0$ . The consequences of this fact will be discussed briefly in Sec. 4.8. We will note, however, that Hartl and others recommend that the spin parameter satisfy  $S \leq 10^{-4} mM$  (see Ref. [14] and references therein)—for such small spins, the effect of enforcing  $p_\mu S^{\mu\nu}$  should also be relatively minor, but nevertheless wrong for orbits generated using the approach we have outlined.

### 4.2.3 Decoupled Orbits

Finally, we can treat the particle as a freely precessing gyroscope by decoupling the spin effects from the motion. In particular, we set  $\dot{E} = \dot{L}_z = \dot{Q} = 0$  but continue to allow the spin to evolve—the particle does not stray from geodesic motion. As such, the total spin should be exactly constant,

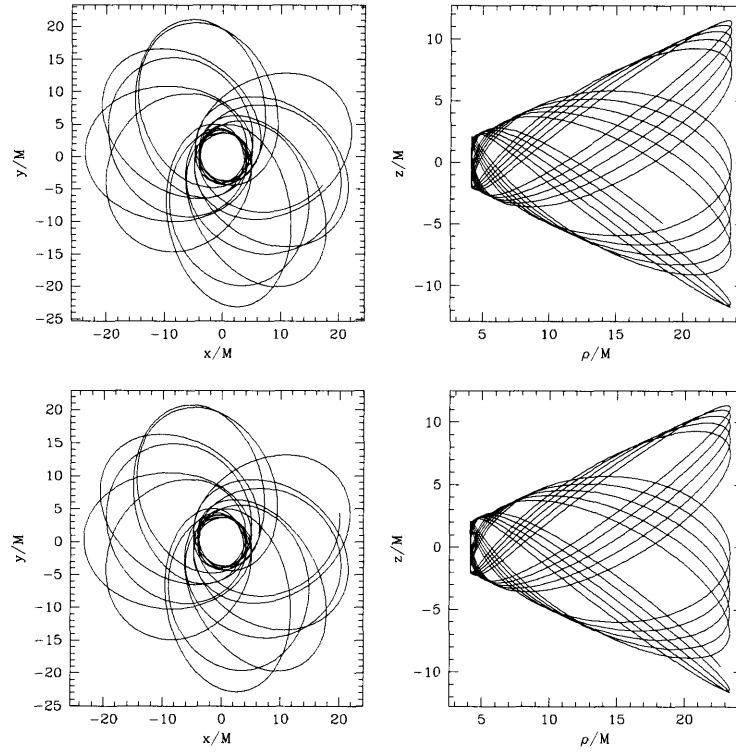


Figure 4-1: This figure illustrates a typical spin-enhanced orbit around a black hole with  $a = 0.9 M$  along with its corresponding geodesic. The parameters for both orbits were  $p = 7 M$ ,  $e = 0.7$ ,  $\iota = 30^\circ$ , and  $S = 10^{-2} m M$ , with the spin oriented in the  $\theta$  direction. Top, left: Projection of the spin-enhanced orbit into the equatorial plane. Top, right: The vertical motion characterizing the spin-enhanced motion orbit. Here,  $\rho$  is the equatorial component of  $r$ , defined by  $\rho = \sqrt{x^2 + y^2}$ . Bottom: Orbital parameters are identical to the top two frames, except that  $S = 0$ , so the motion is geodesic. Notice that the orbits remain virtually indistinguishable even after  $5000 M$  of time, which marks the end of the simulations.

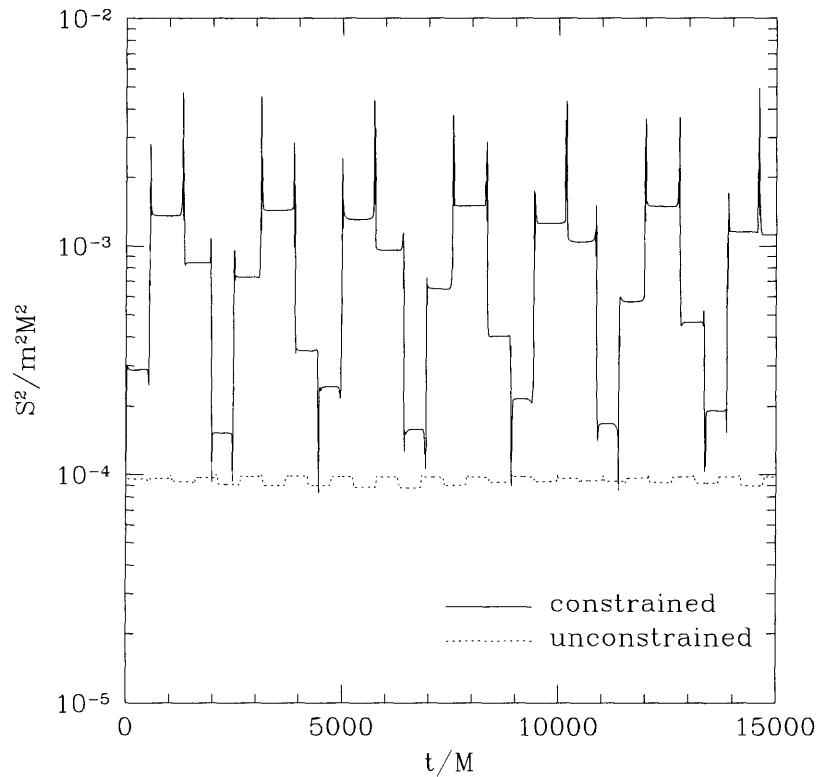


Figure 4-2: The time dependence of  $S^2$  for constrained and unconstrained orbits characterized initially by  $p = 3.35 M$ ,  $e = 0.9$ , and  $\iota = 30^\circ$  around a black hole with  $a = 0.99 M$ . The spin is oriented initially in the outward radial direction with  $S = 10^{-2} mM$ . The variations of  $S^2$  are much smaller when the six spin tensor components are allowed to evolve freely. When we impose the constraint  $p_\mu S^{\mu\nu} = 0$  to eliminate three of the six spins, we observe unacceptably large variations in  $S^2$ .

even as the individual spin tensor components evolve. This will allow us to simultaneously test every derivative in the code except those for  $E$ ,  $L_z$ , and  $Q$ . In other words,  $S^2$  will be conserved only if both the geodesic part of the code and the derivatives of the spin tensor components are working properly. Choosing a relatively extreme orbit allows us to stringently test the accuracy of our equations. Though the individual components of the spin tensor vary with time as they should (see Fig. 4-3), the square of the total spin is indeed perfectly conserved for the entirety of the simulation (which runs to  $15000 M$ ).

### 4.3 Example Orbits

One of the important lessons to be learned through this analysis is that the spin-enhanced orbits appear almost identical to geodesic orbits, even for fairly large values of  $S$  (see Fig. 4-1). With the addition of spin, however, interesting effects are seen in the orbital “constants” (see Fig. 4-4). Note specifically that the constants vary on orbital timescales, but that the fractional variation of each quantity is relatively small. Also notice the quasi-periodic variation of the constants, which is in itself an interesting result. That  $p$ ,  $e$ , and  $\iota$  (or for that matter,  $E$ ,  $L_z$ , and  $Q$ , since one can easily transform between these two sets of constants) exhibit no secular drift, or perhaps more surprisingly, a near-constant amplitude of oscillation, implies that the volume these orbits will occupy in phase space is finite. In other words, the orbit will not follow some unconstrained trek through the space  $(p, e, \iota)$ ; since each of the three parameters can exist only within a fixed range, the size of explorable volume in phase space is limited.

### 4.4 Spin Orientation and Energy Splitting

The gravitational potential is modified by the existence of small body spin—specifically, the spin of the particle couples to the curvature of the background spacetime to produce a measurable difference in the orbital trajectory. Thus far, we have been picturing this interaction in much the same way as the interaction of a magnetic dipole in an external electromagnetic field (albeit with an overall sign difference—gravity is attractive for like “charges”). Specifically, different alignments of the small body spin vector relative to the spin axis of the black hole will produce different energy characteristics, and it is this behavior that we explore in this section. What is important in this analysis is the radial position very early on in the integration; if the radial coordinate at early times is less than that of the corresponding geodesic, the particle is attracted to the black hole. Conversely, if the radial coordinate is greater, the particle is repelled.

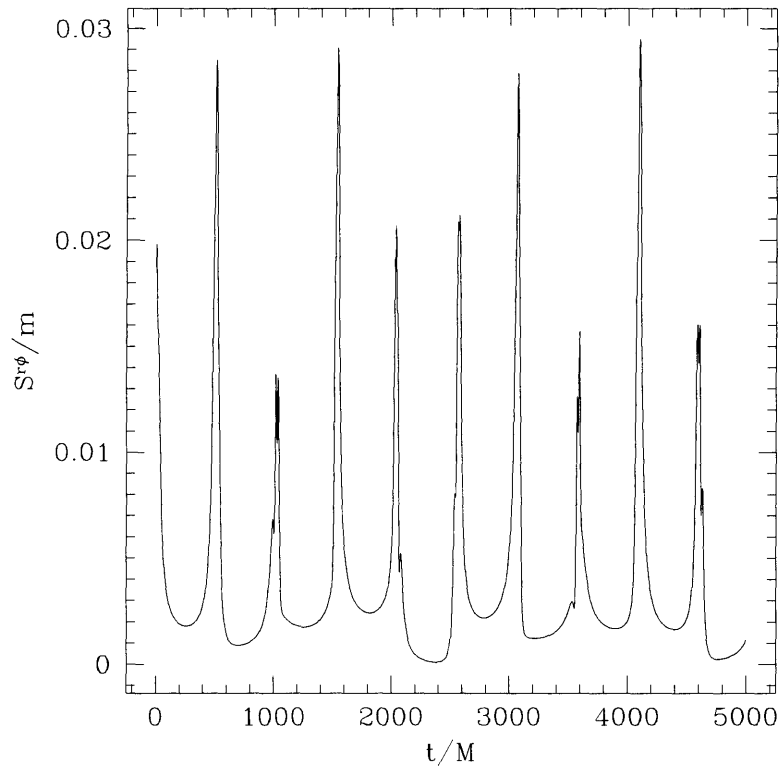


Figure 4-3: The  $S^{r\phi}$  component of the spin tensor evolves along the orbit, as do the other components. This particular orbit is characterized by  $a = 0.9M$ ,  $p = 3M$ ,  $e = 0.9$ , and  $\iota = 20^\circ$ . The spin vector  $\vec{S}$  has equal spatial one-form components, so  $S_r = S_\theta = S_\phi$ . The magnitude of the spin is  $S = 0.1mM$ .

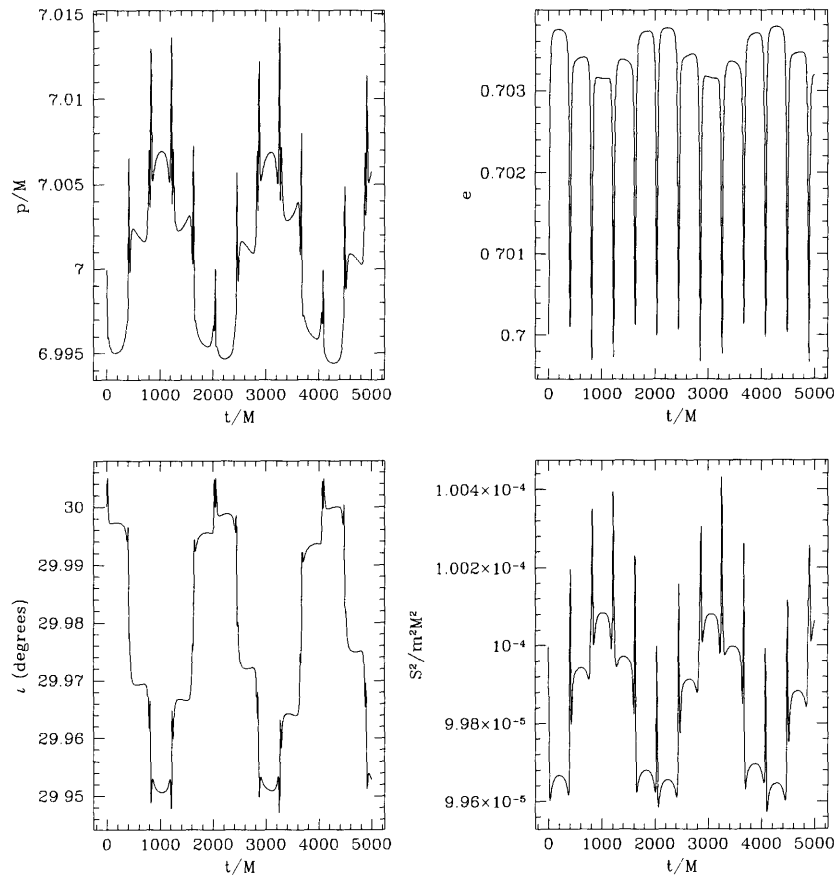


Figure 4-4: This figure contains various “constants” for the spin-enhanced orbit described in Fig. 4-1. Whereas these quantities are indeed true constants in the case of geodesic motion, the introduction of spin causes these quantities to vary on orbital time scales. The variation of the constants is small enough, however, that we can justify treating each of them as legitimate constants in the equations of motion. Counterclockwise from top, left: The semilatus rectum, eccentricity, magnitude squared of the total spin, and inclination angle.

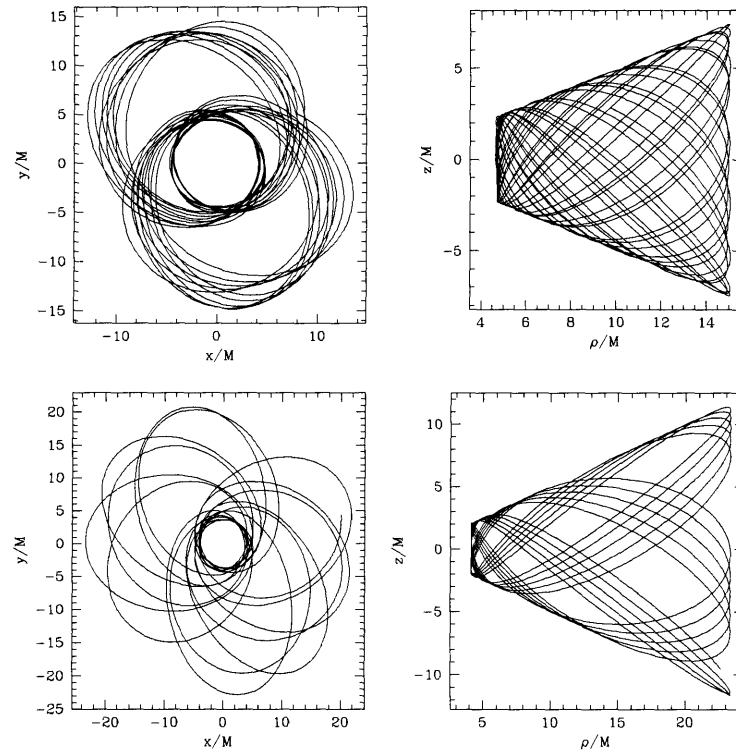


Figure 4-5: This figure compares the behavior of an orbit with  $S = 0.1 mM$  with the corresponding geodesic. The parameters are the same as those in Fig. 4-1 with the exception of  $S$ , which has the same orientation but a different magnitude. Top, left: Projection of the spin-enhanced orbit into the equatorial plane. Top, right: The vertical motion characterizing the spin-enhanced motion orbit. The quantity  $\rho$  is again the equatorial component of  $r$ . Bottom: Orbital parameters are identical to the top two frames, except that  $S = 0$ , so the motion is geodesic. With extremely large values of spin, the variation in the constants of motion is large enough that the orbit trajectory is altered drastically.

#### 4.4.1 Spin in the Polar Direction

There are three basic spatial directions— $\vec{e}_r$ ,  $\vec{e}_\theta$ , and  $\vec{e}_\phi$ —along which the small body spin can be aligned.<sup>1</sup> For orbits with low inclination, spins aligned along  $\vec{e}_\theta$  correspond most closely to what we normally call “spin up” (parallel to  $\vec{S}$ ) and “spin down” (antiparallel to  $\vec{S}$ ).

With the spin aligned with and against  $\vec{e}_\theta$ , the splitting of degenerate trajectories is crystal clear (see Fig. 4-6). If the spins are antiparallel ( $\vec{S}$  is spin down), they attract each other and the particle is held more closely to the black hole than it is along the corresponding geodesic with  $S = 0$ —the antiparallel spin configuration is more tightly bound than the geodesic. This is true of electric and magnetic dipoles as well as quantum spin; the antiparallel, singlet-like configuration is always attractive. The parallel configuration is less tightly bound than the corresponding geodesic, and the particle is repelled.

#### 4.4.2 Spin in the Radial Direction

We can also orient the spin parallel or antiparallel to the radial basis vector  $\vec{e}_r$ . The parallel configuration (“spin out”) is more tightly bound; the particle spends more time closer to the black hole than it does in the antiparallel configuration (“spin in”). Though the distinction between the spin out and spin in states is obvious (see Fig. 4-7), the difference is not as great as it is when the spin is aligned in the polar direction.

#### 4.4.3 Spin in the Azimuthal Direction

Because of the azimuthal asymmetry of a Kerr black hole, prograde ( $+\vec{e}_\phi$ ) and retrograde ( $-\vec{e}_\phi$ ) orbits are not equivalent. There should therefore be evidence of some splitting between prograde and retrograde alignment of spin, and indeed there is. This splitting is illustrated in Fig. 4-8, which shows clearly a spin oriented in the retrograde direction is attracted to the black hole whereas a prograde-oriented spin is repelled.

One important characteristic of this splitting, however, is that it is extremely weak relative to the splitting observed for spins aligned in other directions. The reason for this comparative insignificance is that the splitting of prograde and retrograde orbits is due to the azimuthal symmetry breaking caused by the black hole’s angular momentum, which becomes less significant than other effects at large radii. The splitting will surely be larger for extremely close orbits that venture much deeper into the throat of the black hole spacetime, but will likely always be the weakest of the three splittings.

---

<sup>1</sup>As is conventionally the case, the various  $\vec{e}_\mu$  correspond to basis vectors oriented in the direction of increasing  $x^\mu$ . Also, it should be noted that the actual spin can be oriented in any direction.

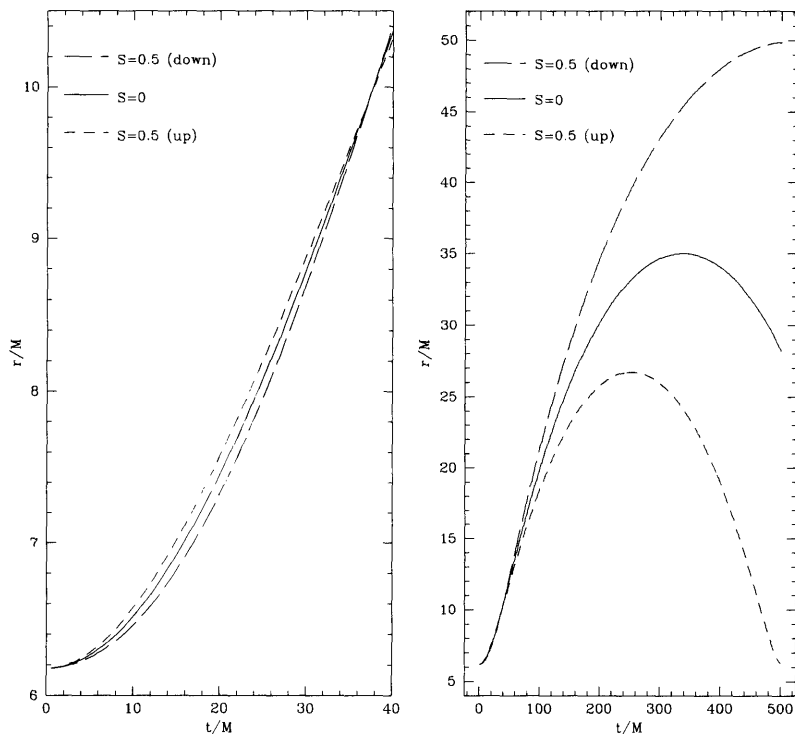


Figure 4-6: The radial position of the particle orbiting a black hole with  $a = 0.9 M$  characterized initially by  $p = 10.5 M$ ,  $e = 0.7$ , and  $\iota = 10^\circ$ . Three different curves are plotted; the middle curve corresponds to the case of no spin on the small body, in which case there is no spin interaction. The other two curves correspond to  $S = 0.5 mM$  pointed parallel or antiparallel to  $\vec{e}_\theta$ . Left: The antiparallel configuration ( $+\vec{e}_\theta$ ) is attractive, and hence is held most closely to the black hole at early times. Right: At later times the ordering switches, and the spin down (antiparallel) particle is located at larger radii. This is probably due to the fact that its attraction to the black hole causes it to spend more time in high-curvature regions of spacetime, which in turn kicks the particle into a more extreme orbit.

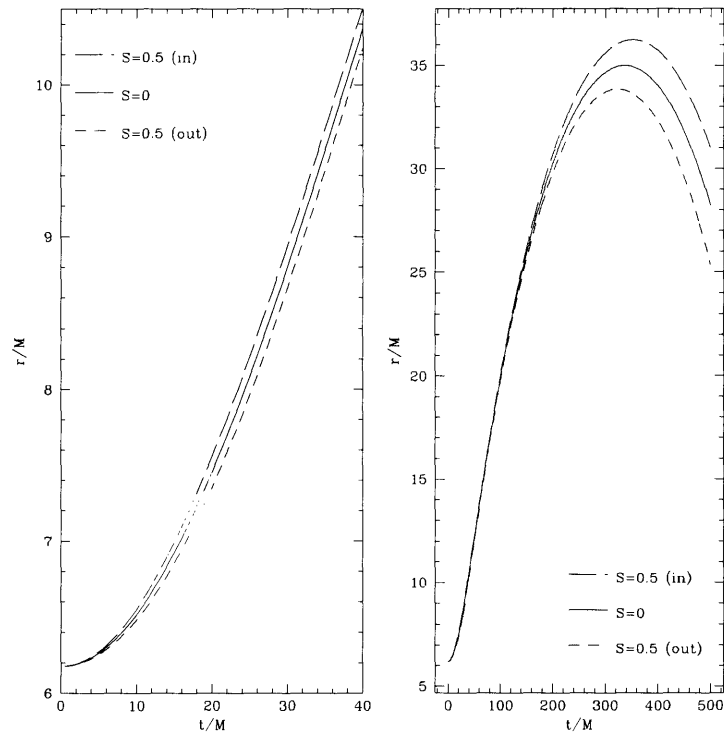


Figure 4-7: The radial position of the particle orbiting a black hole with  $a = 0.9M$  characterized initially by  $p = 10.5M$ ,  $e = 0.7$ , and  $\iota = 10^\circ$ . The middle curve corresponds to the geodesic with  $S = 0$ . The other two curves are both characterized by  $S = 0.5mM$ , but the upper curve and lower curve correspond to the spin in  $(-\vec{e}_r)$  and spin out  $(+\vec{e}_r)$  cases, respectively. The spin out particle is attracted to the black hole. The splitting is not as pronounced as it is when the spin has a polar orientation. Left: The radial coordinate of the particle at early times, indicating the attraction and repulsion of spin out and spin in states, respectively. Right: Radial coordinate over a longer interval.

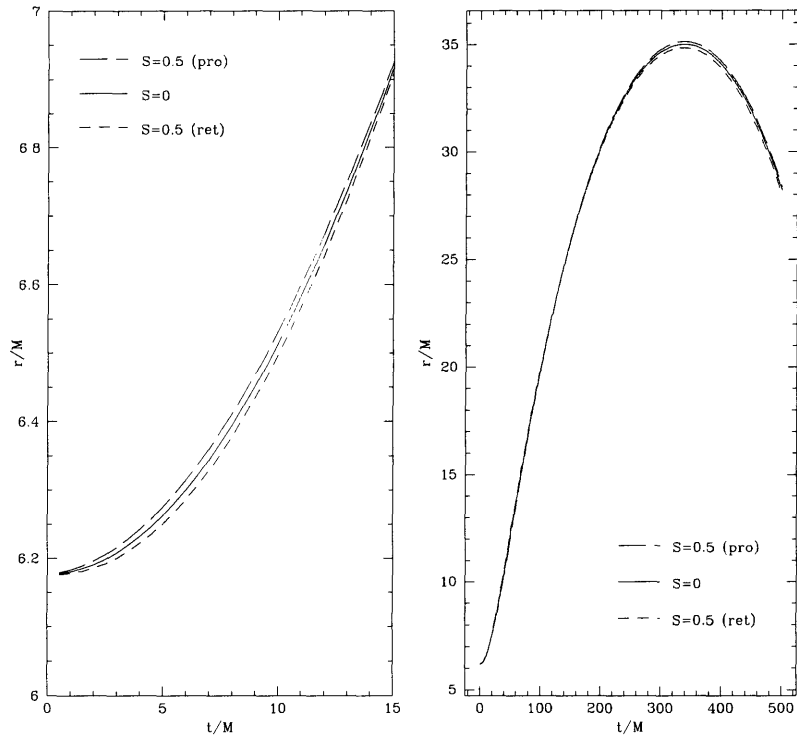


Figure 4-8: The radial position of the particle orbiting a black hole with  $a = 0.9M$  characterized initially by  $p = 10.5M$ ,  $e = 0.7$ , and  $\iota = 10^\circ$ . The middle curve again corresponds to the geodesic with  $S = 0$ . The other two curves are also once again characterized by  $S = 0.5mM$ . The radial position of a retrograde-aligned ( $-e_\phi$ ) spin is initially less than the corresponding geodesic or the prograde-aligned ( $+e_\phi$ ) spin, but the ordering changes twice before the particle reaches apastron. Left: The retrograde-aligned spin is attracted to the black hole while the prograde-aligned spin is repelled. Right: The azimuthal splitting is small because the asymmetries of the Kerr black hole in that direction are not very important beyond about  $r = 3M$ . More extreme orbits may demonstrate a greater amount of splitting.

Table 4.1: Standard deviations of various orbital parameters for an orbit with parameters  $a = 0.5 M$ ,  $p = 7 M$ ,  $e = 0.7$ ,  $\iota = 30^\circ$ , and spin oriented in the positive  $\theta$  direction ( $\vec{e}_\theta$ ). The linearity of  $\sigma_p$ ,  $\sigma_e$ , and  $\sigma_\iota$  with respect to  $S$  is remarkable. The total integration period was  $2000 M$ .

$S/mM$	$\sigma_p/M$	$\sigma_e$	$\sigma_\iota$
0.001	$6.94 \times 10^{-4}$	$1.48 \times 10^{-4}$	$9.19 \times 10^{-6}$
0.005	$3.49 \times 10^{-3}$	$7.38 \times 10^{-4}$	$4.55 \times 10^{-5}$
0.01	$7.01 \times 10^{-3}$	$1.48 \times 10^{-3}$	$9.07 \times 10^{-5}$
0.02	$1.42 \times 10^{-2}$	$2.95 \times 10^{-3}$	$1.80 \times 10^{-4}$
0.03	$2.15 \times 10^{-2}$	$4.43 \times 10^{-3}$	$2.68 \times 10^{-4}$
0.04	$2.90 \times 10^{-2}$	$5.92 \times 10^{-3}$	$3.55 \times 10^{-4}$
0.05	$3.67 \times 10^{-2}$	$7.40 \times 10^{-3}$	$4.41 \times 10^{-4}$
0.1	$7.07 \times 10^{-2}$	$1.33 \times 10^{-2}$	$8.65 \times 10^{-4}$

## 4.5 Variation of Orbital Constants

### 4.5.1 Amplitude of Variation

The size of the variation is necessarily a function of  $S$ . When  $S = 0$ , the scale of the variation should be zero. When  $S$  grows, so too does the variation. It is the goal of this section to uncover the dependence of the variational amplitude on the size of the spin parameter.

To quantify the scale of the variation, we integrate different orbits for a total time of  $2000 M$  and from these simulations compute the standard deviation ( $\sigma$ ) of  $p$ ,  $e$ , and  $\iota$ . The standard deviation should yield a fairly unbiased estimate of the distribution of each quantity, certainly much better than naively computing the range. The integration time of  $2000 M$  was chosen to be much greater than the orbital timescales.

When we proceed with this analysis, we find an obvious linear relationship between the various  $\sigma$  and  $S$ ; the amplitude of variation scales perfectly with the magnitude of the spin. The data for two typical runs are presented in Tables 4.1 and 4.2. One can check that the results do indicate a linear relationship, and that they also make sense in the known limit  $S \rightarrow 0$ , for which the variation amplitude must vanish entirely. Figure 4-9 illustrates that  $\sigma_p/M$  behaves in exactly this way, though the relationship between  $\sigma$  and  $S$  is equally true for the other orbital constants.

### 4.5.2 Frequency Components

The constants—whether they be  $p$ ,  $e$ , and  $\iota$  or  $E$ ,  $L_z$ ,  $Q$ —vary quasi-periodically. Though the actual behavior of each quantity is complicated, they each appear to exhibit strong frequency components matching the radial and polar frequencies of the orbit (see Fig. 4-10). This confirms our previous assertions that  $p$ ,  $e$ , and  $\iota$  vary on orbital timescales. Coupled with the knowledge that the orbital constants exhibit no secular drift, it also provides a good indication that the timescale of the total spin effect is itself similar to the orbital timescale. We will revisit this issue in Sec. 4.7.

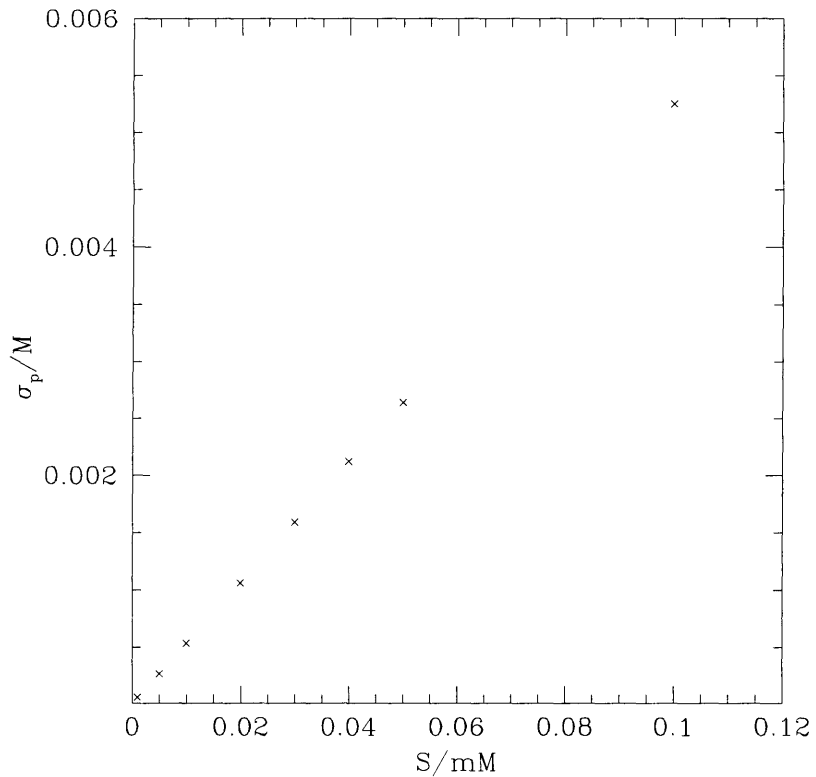


Figure 4-9: The variation amplitude as a function of  $S$  for an orbit characterized by  $a = 0.9 M$ ,  $p = 10 M$ ,  $e = 0.2$ , and  $\iota = 10^\circ$ . The spin was oriented initially along  $\vec{e}_\theta$ . In addition to illustrating the linear relationship between  $\sigma_p$  and  $S$  (indeed, the variation amplitude of the other quantities demonstrate the same linear dependence on  $S$ ), the figure suggests the correct result in the limit  $S \rightarrow 0$ , wherein geodesic motion is recovered and the orbital constants do not oscillate at all.

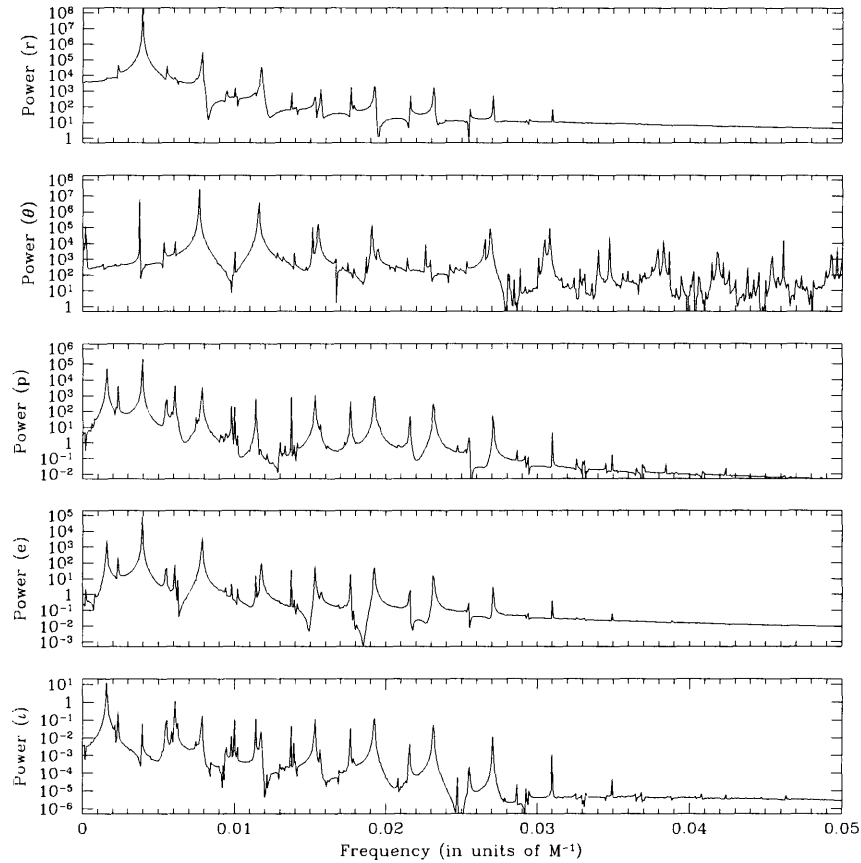


Figure 4-10: The power spectra of various quantities during a typical orbit. Power is defined as the magnitude squared of the complex amplitude. The parameters for the orbit were  $a = 0.3 M$ ,  $p = 7 M$ ,  $e = 0.2$ ,  $\iota = 30^\circ$ , and  $S = 0.1$  pointed in the direction of  $\vec{e}_\theta$ . From top to bottom: radius ( $r$ ), polar angle ( $\theta$ ), semilatus rectum ( $p$ ), eccentricity ( $e$ ), and inclination ( $\iota$ ). Note the strong correlation between the peaks in the  $r$  and  $\theta$  power with the peaks in the  $p$ ,  $e$ , and  $\iota$  power. This indicates that the variations in the “constants” are coming primarily at the orbital timescales. The correlation persists even when the spin orientation is altered or when the orbits are made more extreme by increasing  $a$ ,  $e$ , or  $\iota$  or by decreasing  $p$  toward  $p_{LSO}$ .

Table 4.2: Standard deviations of various orbital parameters for an orbit with parameters  $a = 0.9 M$ ,  $p = 10 M$ ,  $e = 0.2$ ,  $\iota = 10^\circ$ , and spin oriented in the positive  $\theta$  direction ( $\hat{e}_\theta$ ). The integration time was again  $2000 M$ . The superb linearity of  $\sigma_p$ ,  $\sigma_e$ , and  $\sigma_\iota$  persists.

$S/mM$	$\sigma_p/M$	$\sigma_e$	$\sigma_\iota$
0.001	$6.08 \times 10^{-5}$	$6.41 \times 10^{-5}$	$4.43 \times 10^{-6}$
0.005	$2.69 \times 10^{-4}$	$3.20 \times 10^{-4}$	$2.21 \times 10^{-5}$
0.01	$5.35 \times 10^{-4}$	$6.40 \times 10^{-4}$	$4.42 \times 10^{-5}$
0.02	$1.06 \times 10^{-3}$	$1.28 \times 10^{-3}$	$8.85 \times 10^{-5}$
0.03	$1.59 \times 10^{-3}$	$1.91 \times 10^{-3}$	$1.33 \times 10^{-4}$
0.04	$2.12 \times 10^{-3}$	$2.56 \times 10^{-3}$	$1.78 \times 10^{-4}$
0.05	$2.64 \times 10^{-3}$	$3.19 \times 10^{-3}$	$2.23 \times 10^{-4}$
0.1	$5.25 \times 10^{-3}$	$6.36 \times 10^{-3}$	$4.53 \times 10^{-4}$

## 4.6 Phase Space Volume

One of the consequences of the fact that  $p$ ,  $e$ , and  $\iota$  oscillate with near-constant amplitude is that the orbit in phase space is bounded by a fixed and finite volume. As a consequence, the entire orbit must fall within a cuboid defined by the maximum and minimum values of  $p$ ,  $e$ , and  $\iota$  (or  $E$ ,  $L_z$ , and  $Q$ , if one wishes to examine that set of parameters instead). If there are correlations between the parameters, the actual occupied volume will be much smaller than the surrounding cuboid.

Because the amplitude of the variation in  $p$ ,  $e$ , and  $\iota$  scales with  $S$ , we can reasonably expect the volume to grow according to a power law in  $S$ . We do not know *a priori* that the volume scaling will be  $S^3$ . Though unlikely, perfect correlation between the parameters can potentially slow the growth down to linear order in  $S$ . Conversely, the volume can even grow slightly faster than  $S^3$  if the variation in one of the parameters induces greater than normal variation in another one or both of the other parameters.

Before proceeding, we must clarify what we mean when we refer to a trajectory occupying a volume. A trajectory through such a space is defined by a curve, and curves technically do not have volume—they constitute sets of measure zero. We can get around this problem by borrowing a standard technique from computational geometry which involves the creation of a *convex hull*. In physical terms, one can think of a convex hull as the shape generated by wrapping a rubber sheet around a space filled with points and allowing the rubber sheet to contract. The sheet then adopts the smallest possible volume around the points while maintaining its convexity. It is the volume of the region enclosed by each convex hull that we refer to as the phase space volume. Construction and volume estimation of each convex hull is achieved via the quickhull algorithm, described in Ref. [22].

### 4.6.1 Volume Growth with Spin

As we have discussed, we expect the volume to grow roughly as a power law in spin. Hence,

$$V(S) = AS^k, \quad (4.1)$$

where  $k$  is a number and  $A$  is approximately constant. We construct a log – log plot of  $V$  versus  $S$  for a particular orbit in Fig. 4-11. The high degree of linearity evident in the figure indicates that the volume does in fact grow as a power law. The exponent can be inferred from the slope of the plot; its numerical value turns out to be about  $k = 3.1$ . Looking closely at the points, one can make out a slight positive curvature, which suggests that  $A$  itself depends on  $S$ , albeit very mildly.

### 4.6.2 Volume Growth with Semilatus Rectum

The volume increases rapidly as  $p$  decreases toward  $p_{\text{LSO}}$  (see Fig. 4-12). In fact, the volume growth is even faster than exponential. This trend is consistent until the particle gets within a threshold distance of the separatrix, at which point the volume begins to fall and eventually stabilizes. The fundamental reason for this downturn in volume near the separatrix is not immediately clear.

The dependence of volume on  $e$  and  $\iota$  appears to be consistent with the notion that volume grows as one nears the separatrix. Specifically, increasing either  $\iota$  or  $e$  pushes  $p_{\text{LSO}}$  closer to  $p$ , thereby increasing the volume in phase space.

## 4.7 Outlook

One of the most interesting and potentially significant directions in which we intend to push this analysis is toward a direct comparison of the timescales on which spin effects and radiation reaction effects take their toll. Specifically, we plan to compute timescale required for spin effects to drive the orbit until it completely fills the phase space volume, and compare these numbers to those for radiation reaction.

### 4.7.1 Radiation Reaction Timescales

The timescale on which radiation reaction is known analytically. To zeroth order in  $e$ , the timescale required for gravitational radiation reaction to significantly alter the orbit of an orbiting body is given by

$$\tau_{rr} = \frac{\omega}{\dot{\omega}} = \frac{5}{96} \frac{(\mu_1 + \mu_2)^{1/3}}{\mu_1 \mu_2} \omega^{-8/3}, \quad (4.2)$$

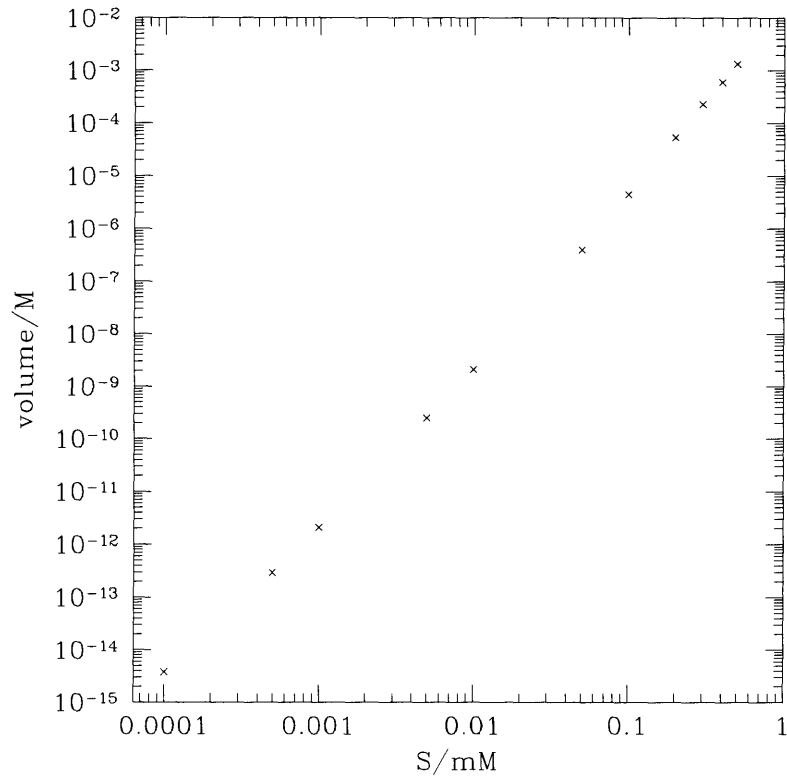


Figure 4-11: Growth of occupied volume in phase space versus  $S$  for an orbit with  $a = 0.9M$ ,  $p = 7M$ ,  $e = 0.7$ ,  $\iota = 15^\circ$ , and spin oriented in the direction of  $\vec{e}_\theta$ . The growth is such that  $V(S) \approx AS^{3.1}$ . Close inspection will reveal slight positive curvature to the points, indicating the weak dependence of  $A$  on  $S$ .

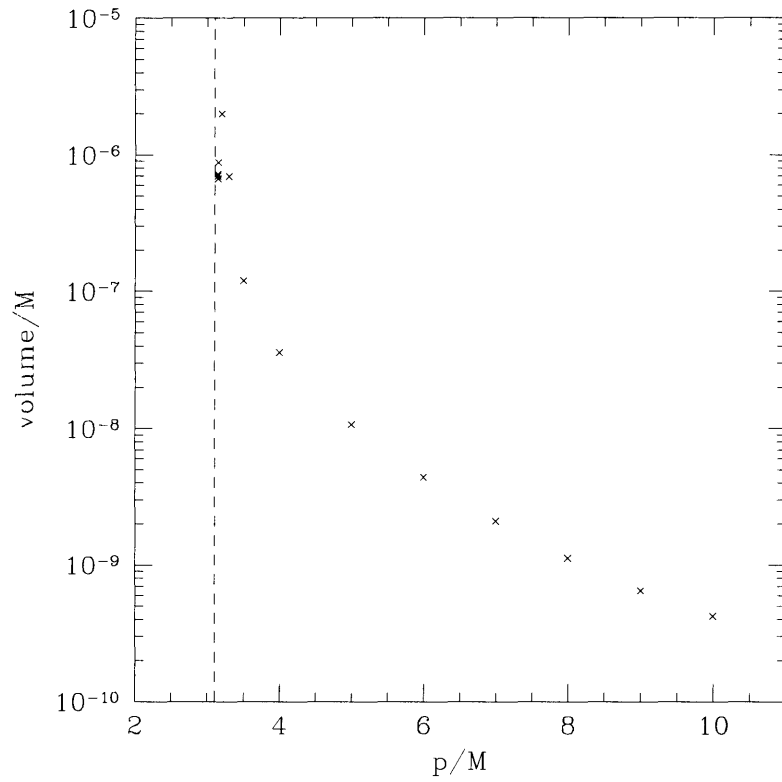


Figure 4-12: Growth of occupied volume in phase space versus  $p$  for an orbit with  $a = 0.9 M$ ,  $e = 0.7$ ,  $\iota = 15^\circ$ , and spin oriented in the direction of  $\vec{e}_\theta$  with magnitude  $S = 0.01 M$ . The dashed line indicates the separatrix between stable and unstable orbits at  $p_{\text{LSO}} = 3.14254 M$ . Note the interesting downturn in the volume as one gets very close to  $p_{\text{LSO}}$ .

where  $\mu_1$  and  $\mu_2$  are the masses of the bodies. Setting  $\mu_1 = m$  and  $\mu_2 = M$  and using Kepler's Law, we find

$$\omega = \sqrt{\frac{m+M}{r^3}}, \quad (4.3)$$

which implies

$$\frac{\tau_{rr}}{M} = \frac{5}{96} \frac{(r/M)^4}{(1+m/M)(m/M)}. \quad (4.4)$$

We can directly compare this last result to the spin timescales by recalling that  $S = m/M$  for a maximally spinning particle. Accordingly,

$$\frac{\tau_{rr}}{M} = \frac{5}{96} \frac{(r/M)^4}{(1+S)S}. \quad (4.5)$$

The timescale differs by as much as a factor of five when one considers eccentricity, but nonetheless provides a relatively good indication of the actual timescale.

#### 4.7.2 Radiation Reaction versus Spin

The purpose of comparing radiation reaction and spin timescales is to understand which effect “wins” in real systems. Specifically, spin tends to spread nearby trajectories apart, albeit slightly, whereas radiation reaction tends to drive them together.

What is interesting to note about Eq. (4.5) is that the timescale decreases uniformly as  $S$  increases. For very small  $S$ ,  $\tau_{rr}$  is quite large. Preliminary testing of the spin timescales suggests that the opposite trend may be true for spin. In particular, since the total occupied volume of phase space grows fairly quickly with  $S$ , it takes a greater amount of time for the particle to fill the space—the timescale seems to *increase* with increasing  $S$ . The implication is obvious; we may be able to cause the spin timescale to be smaller than the radiation reaction timescale by choosing  $S$  that is sufficiently small. This tantalizing result will be explored in upcoming work.

### 4.8 Outstanding Issues

As we mentioned before, the center of mass constraint,  $p_\mu S^{\mu\nu} = 0$ , pinpoints the particle's mass center. Because the constraint  $p_\mu S^{\mu\nu} = 0$  is violated—albeit by a small amount—in the full evolution, there remains a question about the position of the center of mass. Such a mass center is sure to exist, but the best we can do is to say that it has been localized to within some small region. This does not appear to pose a problem as far as our simulations are concerned, but it does appear unnerving from the standpoint of theory. As of yet, we are not sure what to make of this apparent

underdetermination of an important property of the orbiting particle.



# Bibliography

- [1] Robert M. Wald, editor. *Black Holes and Relativistic Stars*. Univ. Chicago Press, 1998.
- [2] John Kormendy and Douglas O. Richstone. Inward Bound: The Search for Supermassive Black Holes in Galactic Nuclei. *Ann. Rev. Astron. Astrophys.*, 33:581–624, 1995.
- [3] John Kormendy. The Stellar-Dynamical Search for Supermassive Black Holes in Galactic Nuclei. 2003.
- [4] Steinn Sigurdsson and Martin J. Rees. Capture of Stellar-Mass Compact Objects by Massive Black Holes in Galactic Cusps. *Mon. Not. R. Astron. Soc.*, 284:318–326, 1997.
- [5] Steinn Sigurdsson. Estimating the Detectable Rate of Capture of Stellar Mass Black Holes by Massive Central Black Holes in Normal Galaxies. *Class. Quant. Grav.*, 14:1425–1429, 1997.
- [6] Subrahmanyan Chandrasekhar. *The Mathematical Theory of Black Holes*. Oxford University Press, New York, 1983.
- [7] Saul A. Teukolsky. Rotating Black Holes—Separable Wave Equations For Gravitational And Electromagnetic Perturbations. *Phys. Rev. Lett.*, 29:1114–1118, 1972.
- [8] Saul A. Teukolsky. Perturbations of a Rotating Black Hole. 1. Fundamental Equations for Gravitational Electromagnetic, and Neutrino Field Perturbations. *Astrophys. J.*, 185:635–647, 1973.
- [9] Misao Sasaki and Takashi Nakamura. Gravitational Radiation from a Kerr Black Hole. I — Formulation and a Method for Numerical Analysis—. *Prog. Theor. Phys.*, 67:1788–1809, 1982.
- [10] Sean M. Carroll. *Spacetime and Geometry: An Introduction to General Relativity*. Pearson Addison Wesley, San Francisco, 2003.
- [11] Charles W. Misner, Kip S. Thorne, and John A. Wheeler. *Gravitation*. Freeman, San Francisco, 1973.
- [12] Achilles Papapetrou. Spinning Test-Particles in General Relativity, I. *Proc. R. Soc. London*, A209:248–258, 1951.

- [13] William G. Dixon. Dynamics of Extended Bodies in General Relativity. I. Momentum and Angular Momentum. *Proc. R. Soc. London*, A314:499–527, 1970.
- [14] Michael D. Hartl. *Dynamics of Spinning Compact Binaries in General Relativity*. PhD dissertation, California Institute of Technology, Department of Physics, 5 2003.
- [15] Scott A. Hughes and Teviet D. Creighton. Dynamics of Generic Kerr Black Hole Orbits: Notes and Homework Assignments.
- [16] Kostas Glampedakis and Daniel J. Kennefick. Zoom and whirl: Eccentric equatorial orbits around spinning black holes and their evolution under gravitational radiation reaction. *Phys. Rev.*, D66:044002, 2002.
- [17] Daniel C. Wilkins. Bound Geodesics in the Kerr Metric. *Phys. Rev.*, D5:814–822, 1972.
- [18] William H. Press, Brian P. Flannery, Saul A. Teukolsky, and William T. Vetterling. *Numerical Recipes in C: The Art of Scientific Computing*. Cambridge University Press, 1992.
- [19] James M. Bardeen, William H. Press, and Saul A. Teukolsky. Rotating Black Holes: Locally Nonrotating Frames, Energy Extraction, and Scalar Synchrotron Radiation. *Astrophys. J.*, 178:347–370, 1972.
- [20] Scott A. Hughes. The Evolution of Circular, Non-Equatorial Orbits of Kerr Black Holes due to Gravitational-Wave Emission. *Phys. Rev.*, D61:084004, 2000.
- [21] Takahiro Tanaka, Yasushi Mino, Misao Sasaki, and Masaru Shibata. Gravitational Waves from a Spinning Particle in Circular Orbits around a Rotating Black Hole. *Phys. Rev.*, D54:3762–3777, 1996.
- [22] David P. Dobkin C. Bradford Barber and Hannu T. Huhdanpaa. The Quickhull Algorithm for Convex Hulls. *ACM Trans. on Mathematical Software*, 22(4):469–483, December 1996.